FAM13A regulates maturation and effector functions of natural killer cells

Ni Zeng[1,2], Maud Theresine[1], Christophe Capelle[1,2], Neha Patil[1,2], Cécile Masquelier[1], Caroline Davril[1], Alexander Baron[1], Djalil Coowar[3], Xavier Dervillez[1], Aurélie Poli[1], Cathy Leonard[1], Rudi Balling[3], Markus Ollert[1,4], Jacques Zimmer[1*] and Feng Q. He[1,3,5*]

1, Department of Infection and Immunity, Luxembourg Institute of Health (LIH), 29, rue Henri Koch, Esch-sur-Alzette, L-4354, Luxembourg;
2, Faculty of Science, Technology and Medicine, University of Luxembourg, 2, avenue de l'Université, Esch-sur-Alzette, L-4365, Luxembourg;
3, Luxembourg Centre for Systems Biomedicine (LCSB), University of Luxembourg, 6, avenue du Swing, Belvaux, L-4367, Luxembourg;
4, Department of Dermatology and Allergy Center, Odense Research Center for Anaphylaxis (ORCA), University of Southern Denmark, Odense, 5000 C, Denmark;
5, Institute of Medical Microbiology, University Hospital Essen, University Duisburg-Essen, D-45122 Essen, Germany
*Correspondence should be addressed to J.Z. (jacques.zimmer@lih.lu) or F.Q.H. (feng.he@lih.lu).

Abstract

The education or licensing process is essentially required for the proper anti-tumor function of natural killer (NK) cells. Although several models for education have been proposed, the genetic factors regulating these processes still remain largely elusive. Here we show that FAM13A (family with sequence similarity 13, member A), strongly linked to the risk of prominent death-causing lung diseases, i.e., lung cancer and chronic obstructive pulmonary disease, critically modulated NK cell maturation and effector functions. *Fam13a* depletion promoted NK cell maturation, KLRG1 (killer cell lectin-like receptor G1) expression in NK cells and NK terminal differentiation in homeostatic mice. NK cells from *Fam13a*-deficient mice had impaired IFN-γ production and degranulation. Strikingly, the number of lung metastases induced by B16F10 melanoma cells was increased in *Fam13a*-deficient mice. Collectively, our data reveal a pivotal role of FAM13A in slowing down NK maturation, but promoting NK cell effector functions and immune protection against tumor metastasis.

Keywords

FAM13A; Natural killer cells; Lung cancer; IFN-γ; Degranulation; NK maturation; NK education.

Number of Characters

39,196 (including space, main text without Abstract)

Introduction

The functions of natural killer (NK) cells are governed through a panel of germline-encoded activating (AR) and inhibitory (IR) receptors (Caligiuri 2008, Demaria et al. 2019). The balance of signals transmitted through these receptors determines the fate of the target cells, which are killed when the activation prevails over the inhibition but spared when the contrary is the case. However, this balance is not enough to render NK cells functional: they must, in addition, be "licensed" or "educated". This education process takes place when a developing NK cell expressing an IR specific for an autologous major histocompatibility complex (MHC) class I molecule in the microenvironment interacts with this structure (He and Tian 2017, Boudreau and Hsu 2018). The consequence is that a NK cell is able to efficiently detect diseased cells that have downregulated their MHC class I expression (such as cancer cells and infected targets), without killing healthy cells. In human, these IR are mainly the killer immunoglobulin-like receptors (KIR) and the C-type lectin CD94/NKG2A, whereas the mouse counterparts are the Ly49 family and the mouse orthologue of human NKG2A is also present. In parallel, several MHC class I-independent IR have likewise been described to educate NK cells (He and Tian 2017). A seminal work has demonstrated the licensing concept in mice by showing that Ly49C^{+} NK cells, specific for the MHC class I ligands H-2K^{b} and H-2D^{b} present in C57BL/6 (B6) mice, are better licensed than the Ly49C^{-} cells from the same individuals (Kim et al. 2005). The same work also reported that upon short activation with the TLR3 agonist poly I/C or stimulation by the cytokine interleukin (IL)-2, the difference between the two subsets becomes less pronounced but is still present (Kim et al. 2005).

We aimed to get further insight into this topic, because in immunotherapeutic approaches with human activated autologous or allogeneic NK cells, it might be of advantage to select those that are best educated and therefore most efficient in tumor cell killing. For this purpose, we included for simplicity the known MHC class I specific IR expressed by NK cells from the B6 (H-2^{b}) background, namely Ly49C (ligands: H-2K^{b}, H-2D^{b}), Ly49I (same ligands), and NKG2A (ligand: Qa-1^{b}, the mouse orthologue of HLA-E, presenting signal peptides derived from the classical MHC class I molecules,

which are H-2D^b and H-2K^b in B6 mice) (Boudreau and Hsu 2018). In contrast to the other works mainly based on resting or short-term or IL-2-stimulated NK cells (Kim et al. 2005), we here investigated the education process of the four subsets defined by the combinatory expression of NKG2A and Ly49I/C using different stimulation conditions with various cytokine cocktails. Those cytokine cocktails versus (vs.) IL-2 alone better mimic the tumor microenvironment. Furthermore, since the involvement of the immune system, and particularly of NK cells, in the fight against tumor genesis and metastasis is crucial (Vesely et al. 2011, Zimmer 2014, Cerwenka and Lanier 2016, Janssen et al. 2017, Huntington et al. 2020), we sought to identify and investigate whether a novel candidate gene, which is known to be associated with the risk of lung tumors, regulates the education process of NK cells. This is rationale as profound phenotypic and functional alterations of NK cells have been shown in lung cancer (Al Omar et al. 2011, Platonova et al. 2011, Cong and Wei 2019, Hervier et al. 2019) and particularly, in non-small cell lung cancer, several specific KIR genes are associated with better treatment response and longer survival (Kusnierczyk 2013).

Meanwhile, to further narrow down the candidate list, we assessed the genes also linked with the risk of another major lung disease, i.e., chronic obstructive lung disease (COPD), the pathogenesis and progression of which NK cells also significantly contribute to (Eriksson Strom et al. 2018, Pascual-Guardia et al. 2020). To this end, the gene FAM13A (family with sequence similarity 13, member A), a well-recognized risk gene, nonetheless less-characterized in the immune system, for both COPD and lung cancer in human came to the center of the study. Several independent genome-wide association studies (GWAS) among various populations have shown the strong link between FAM13A, COPD and lung cancer (Cho et al. 2010, Guo et al. 2011, Young et al. 2011, Wang et al. 2013, Kim et al. 2015, Ziółkowska-Suchanek et al. 2015, Hirano et al. 2017, van der Plaat et al. 2017, Ziółkowska-Suchanek et al. 2017, Zhang et al. 2018, Castaldi et al. 2019, Yu et al. 2019). The polymorphism of FAM13A was also associated with cystic fibrosis (Corvol et al. 2018). Functional studies have revealed that *Fam13a* depletion reduces the susceptibility to COPD via inhibiting the WNT/β-catenin pathway in a mouse model (Jiang et al. 2016). In human lung tumor cell lines, knocking-down FAM13A reduced tumor cell proliferation but induced cell migration *in vitro* (Eisenhut et al. 2017). However, the exact *in vivo*

physiological role of *Fam13a* in the complicated process of tumor onset and metastasis, where different types of cells are heavily involved, still remains mysterious. Furthermore, in the same study, the authors observed the upregulation of FAM13A in $CD4^+CD25^-$ effector T cells but reduced expression in T regulatory cells (Tregs) of human blood. In contrast, in our previous study (He et al. 2012), the expression of FAM13A was increased in human Tregs vs. $CD4^+$ effector T cells. Another work with the expression quantitative trait loci (eQTL) method has briefly investigated the functional effect of FAM13A on naïve $CD4^+$ T cells *in vitro* using siRNA (Schmiedel et al. 2018). Meanwhile, microRNA-328 in M2 macrophage-derived exosomes has been demonstrated to regulate the progression of pulmonary fibrosis via *Fam13a* in an animal model (Yao et al. 2019). We therefore hypothesized that *Fam13a* might also play a vital role in regulating immune functions *in vivo*, although it is still unclear in which types of immune cells.

Here we utilized a *Fam13a* whole-body knockout (KO) mouse model to study the *in vivo* impact of *Fam13a* on NK cell phenotypes and functions, in addition to the cellular phenotypes of T and B lymphocytes. We found that *Fam13a* did not affect the homeostatic composition and activities of total B cells, $CD4^+$ T cells, $CD4^+$ Tregs and $CD8^+$ T cells. Interestingly, *Fam13a* depletion changed the NK cell maturation profile and impaired the effector functions of NK cells by controlling IFN-γ production and degranulation. Notably, *Fam13a* depletion exacerbated lung metastasis induced by B16F10 melanoma cells in the B6 mouse model. Altogether, our results provide strong evidence that *Fam13a* is an important component regulating the effector functions of NK cells, mostly through modulating their maturation and IFN-γ production.

Results

Characterization of the immune phenotpye of *Fam13a* KO mice

To identify the potential effect of *Fam13a* on the homeostatic phenotype of the immune system, we first analysed the composition of different major immune cell types in various lymphoid organs and tissues of *Fam13a* KO mice [$Fam13a^{tm2a\ (KOMP)Wtsi}$] obtained from the Knockout Mouse Project vs. the age- and gender-matched littermate controls (wildtype, WT). As a starting point, we compared the mRNA expression of *Fam13a* in the lung tissue between *Fam13a* KO and WT and that in NK cells isolated

from spleen. As expected, *Fam13a* KO mice relative to WT littermates exhibited a significant reduction in the transcript expression of *Fam13a* in both the lung tissue (**Fig. 1a**) and NK cells (**Fig. 1b**). We checked the frequency of $CD19^{-}CD3^{-}NK1.1^{+}$ NK cells in several relevant tissues including spleen (**Fig. 1c, d**), peripheral lymph nodes (pLNs) (**Extended Data Fig. 1a**), bone marrow (BM) (**Extended Data Fig. 1b**) and lung (**Extended Data Fig. 1c**) and no significant difference between homeostatic *Fam13a* KO and WT mice was observed. We also could not see any significant differences in the frequencies of several other lymphocytes, such as $CD3^{+}$ T cells (**Fig. 1e**), $CD19^{+}$ B cells (**Fig. 1f**), $CD8^{+}$ T cells (**Fig. 1g**), $CD4^{+}$ T cells (**Fig. 1h),** as well as $FOXP3^{+}$ $CD4^{+}$ Treg cells (**Fig. 1i**). We further characterized the naïve and memory compartment of $CD4^{+}$ and $CD8^{+}$ T cells. Again, no significant difference was found for the percentage of naïve ($CD44^{low}CD62L^{high}$) and effector memory ($CD44^{high}CD62L^{low}$, EM) $CD4^{+}$ T cells (**Fig. 1j, k**) and naïve, EM and central memory ($CD44^{high}CD62L^{high}$, CM) $CD8^{+}$ T cells in the tested age (8-12 wks) (**Fig. 1l, m**). In conclusion, *Fam13a* depletion does not lead to spontaneous abnormalities in the development of various major immune cells and no obvious inflammatory symptoms or immunodeficiency were observed in homeostatic *Fam13a* KO mice.

To further evaluate whether *Fam13a* influences the basic functions of those immune cells, we analysed the homeostatic activation and proliferation markers of $CD4^{+}$ and $CD8^{+}$ T cells. No significant differences in the frequency of the $CD69^{+}$ population among $CD4^{+}$ T cells and $CD8^{+}$ T cells in spleen (**Extended Data Fig. 1d, e**) exhibited between *Fam13a* KO and WT mice. For another activation or exhaustion marker, PD-1, we also couldn't find any significant difference in the percentages of PD-1^{+} $CD4^{+}$ and PD-1^{+} $CD8^{+}$ T cells between *Fam13a* KO and WT mice (**Extended Data Fig. 1f, g**). To analyze cell proliferation under homeostasis, we examined Ki-67 expression among $CD4^{+}$ and $CD8^{+}$ T cells. no difference in the percentages of Ki-67-expressing cells was noticed among total $CD4^{+}$ T cells (**Extended Data Fig. 1h**) and among total $CD8^{+}$ T cells (**Extended Data Fig. 1i**) between *Fam13a* KO and WT mice. For Tregs, we evaluated the suppressive function by co-culturing the CFSE-labelled $CD4^{+}$ conventional T cells (Tconv), antigen-presenting cells (APCs) and Tregs. Loss of *Fam13a* did not compromise Treg suppressor function against Tconv proliferation (**Extended Data Fig. 1j**). In short,

Fam13a depletion causes deficiency neither in the development, nor in the activation or proliferation of major lymphoid subsets such as CD4$^+$ and CD8$^+$ T cells, at least in mice under homeostatic conditions.

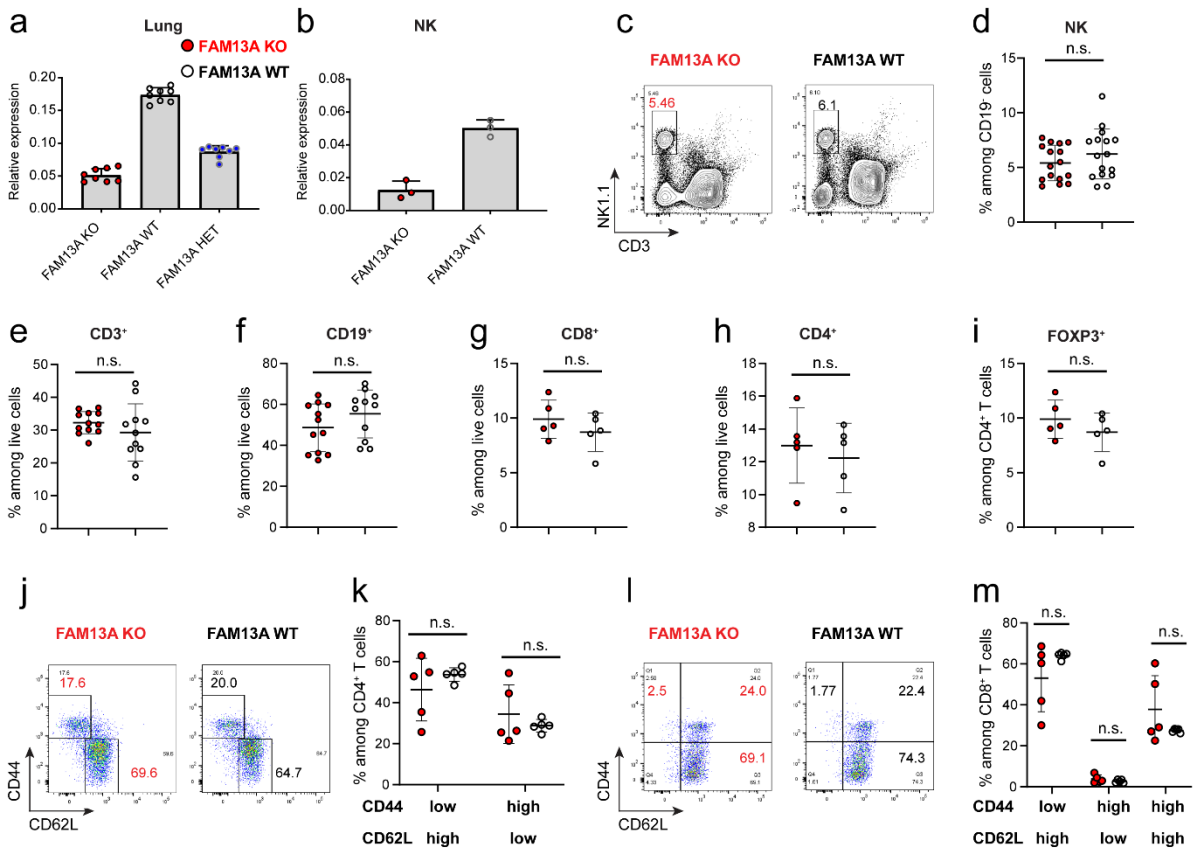

Figure 1. Homeostatic immunophenotyping of *Fam13a* KO mice

a, b, Relative *Fam13a* mRNA expression in lung tissue (**a**) or fresh NK cells (**b**) isolated from *Fam13a* KO or WT littermates or Fam13a heterozygous (HET) mice as quantified by real-time PCR.

c, Representative flow-cytometry (FACS) plots of CD3$^-$ NK1.1$^+$ NK cells among CD19$^-$ cells in spleen of *Fam13a* KO and WT littermates.

d, Percentages of NK cells in spleen (**d**, KO, n= 16; WT, n=16) of *Fam13a* KO and WT littermates.

e, f, g, h, i, Percentages of CD3$^+$ (**e**), of CD19$^+$ B cells (**f**) (KO, n=12, WT, n=11), of CD8$^+$ cytotoxic T cells (**g**), of CD4$^+$ helper T cells (**h**) among the living singlet lymphocytes and percentages of FOXP3$^+$ Tregs among total CD4$^+$ T cells (**i**) in spleen of *Fam13a* KO and WT littermates (KO, n=5, WT, n=5).

j, Representative FACS plot of naïve (CD62L^{high} CD44^{low}) and effector memory (EM) (CD62L^{low} CD44^{high}) T cells among total CD4$^+$ T cells in spleen of *Fam13a* KO and WT littermates.

k, Percentages of naïve and EM CD4$^+$ T cells among total CD4$^+$ T cells in spleen of *Fam13a* KO and WT littermates (KO, n=5, WT, n=5).

l, Representative FACS plot of naïve (CD62L^{high} CD44^{low}), EM (CD62L^{low} CD44^{high}), central memory (CM) (CD62L^{high} CD44^{high}) CD8$^+$ T cells among total CD8$^+$ T cells in spleen of *Fam13a* KO and WT littermates.

m, Percentages of naïve (CD62L^{high} CD44^{low}), EM (CD62L^{low} CD44^{high}), central memory (CM) (CD62L^{high} CD44^{high}) CD8$^+$T cells among total CD8$^+$ T cells in spleen of *Fam13a* KO and WT littermates (KO, n=5; WT, n=5). Results represent two (**a**, **b**), three (**d**, **e**, **f**) and four (**g**, **h**, **i**, **k**, **m**) independent experiments. Data are mean

± standard deviation (s.d.). The *p*-values are determined by a two-tailed Student's t-test. n.s. or unlabeled, not significant, **p*<=0.05, ***p* <=0.01 and ****p* <=0.001.

Fam13a **regulates NK cell maturation**

Similar to T cells, no significance difference was observed in the activation marker CD69 in NK cells in spleen and pLNs between *Fam13a* KO and WT littermates (**Extended Data Fig. 1k, l**). To explore whether *Fam13a* affects other NK cell parameters, we investigated the maturation profile of NK cells by checking the co-expression of CD27 and CD11b. Interestingly, we noticed that *Fam13a* depletion led to a modestly reduced proportion of immature $CD11b^{-}CD27^{+}$ (**Fig. 2a, b**), but significantly increased percentages of mature $CD11b^{+}CD27^{-}$ NK cells (**Fig. 2a, b**). Since $CD11b^{+}CD27^{-}$ NK cells are terminally differentiated NK cells, representing the major KLRG1-expressing NK subset (Huntington et al. 2007, Chiossone et al. 2009, Elpek et al. 2010), we also analyzed the expression of the inhibitory receptor and maturation marker KLRG1 among NK cells. In line with the data related to CD27 and CD11b subsets, we also observed a much higher percentage of KLRG1-expressing cells among total NK cells in both spleen (**Fig. 2c, d**) and pLNs (**Fig. 2e, f**).

We then analyzed another important aspect of the NK functions, i.e., NK cell education which is crucial for the acquisition of its effector properties (Höglund and Brodin 2010). Interestingly, the two Ly49C/I negative subsets among the four subsets defined by the combination of presence or absence of NKG2A and Ly49C/I, the two crucial IR related to education in the C57BL/6 ($H\text{-}2^{b}$) genetic background, represented the major fractions of NK cells in the splenocytes of WT mice (**Fig.2g, h**). *Fam13a* depletion did not cause a significant change in the fraction of any of the four subsets defined by the combinatory expression of NKG2A and Ly49C/I (**Fig. 2g, h**). We also checked the expression of the maturation marker KLRG1 among the four subsets of NK cells in WT spleen and found that KLRG1 was mainly expressed among the two $Ly49C/I^{+}$ subsets (**Fig. 2i**). Notably, again in line with the effect of *Fam13a* on NK cell maturation, a significant upregulation of KLRG1 was observed on several NK subsets, including $NKG2A^{+}Ly49C/I^{+}$, $NKG2A^{-}Ly49C/I^{+}$ and $NKG2A^{-}Ly49C/I^{-}$ NK subpopulations (**Fig. 2i**), but not on the NKG2A single positive cells.

To get a more comprehensive picture, we further analyzed different IR and AR of NK cells, whose engagement is critical to regulate and balance NK cell activities. For the AR, the frequency of NKp46^{+}, Ly49H^{+} and Ly49D^{+} NK cells (**Extended Data Fig. 2a-d**), as well as the expression of 2B4 and NKG2D (**Extended Data Fig. 2e, f**) were not significantly altered in *Fam13a* KO NK cells. For the IR, we did not observe any significant difference in the expression of Ly49A, Ly49C/I and NKG2A (**Extended Data Fig. 2g-i**) on NK cells between *Fam13a* KO and WT mice. In summary, loss of *Fam13a* accelerates the maturation process of NK cells.

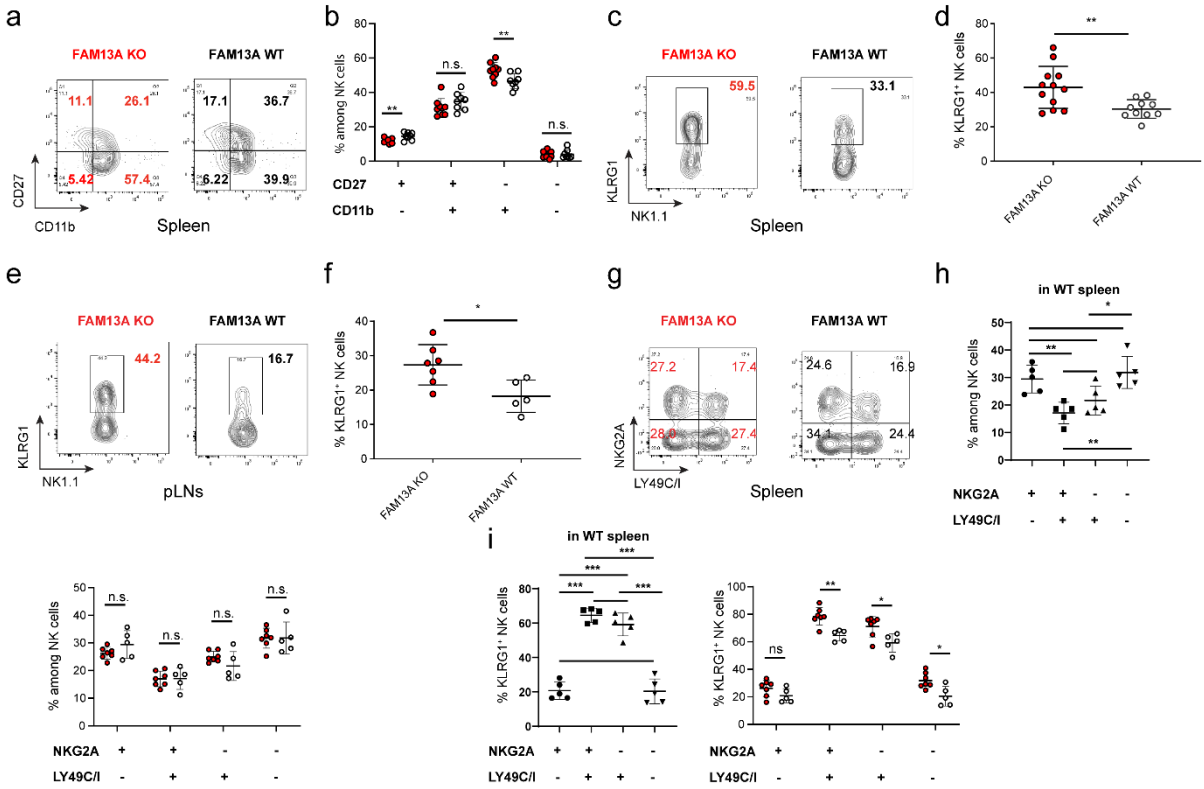

Figure 2. *Fam13a* slows down NK cell maturation

a, Representative FACS plots of CD27 and CD11b expression gated on CD19^{-}CD3^{-} NK1.1^{+}cells in spleen.

b, Percentages of four developmental stages of NK cells, immature CD27^{-}CD11b^{-}, CD27^{+}CD11b^{-}, CD27^{+}CD11b^{+}, CD27^{-}CD11b^{+} mature NK cells in spleen of *Fam13a* KO and WT littermates (KO, n=9; WT, n=8).

c, Representative FACS plots of KLRG1 and NK1.1 expression on CD19^{-}CD3^{-} NK1.1^{+}cells in spleen .

d, Percentages of KLRG1^{+}CD19^{-}CD3^{-}NK1.1^{+} among NK cells in spleen of *Fam13a* KO and WT littermates (KO, n=12; WT, n=10).

e, Representative FACS plots of KLRG1 expression on CD19^{-}CD3^{-} NK1.1^{+}cells in the pLNs of *Fam13a* KO and WT littermates.

f, Percentage of KLRG1^{+} subpopulation among NK cell in pLNs of *Fam13a* KO and WT littermates (KO, n=7; WT, n=5).

g, Representative FACS plots of NKG2A and Ly49C/I expression on CD19^{-}CD3^{-} NK1.1^{+}cells in spleen of *Fam13a* KO and WT littermates.

h, Percentages of four NK cell subpopulations based on the combinatory expression of NKG2A and Ly49C/I IR in spleen of WT (upper panel) as well as *Fam13a* KO vs. WT littermates (lower panel; KO, n=7; WT, n=5).

i, Percentages of KLRG1^{+} cells in NK cell subpopulations in the spleen based on the combinatory expression of NKG2A and Ly49C/I in spleen of WT mice or *Fam13a* KO vs. WT mice (KO, n=7; WT, n=5). Results represent three (**g**, **h**, **i**) and four (**b**, **d, f**) independent experiments. Data are mean±s.d. The p-values are determined by a two-tailed Student's t-test. n.s. or unlabeled, not significant, *p<=0.05, **p<=0.01 and ***p<=0.001. For multiple comparisons, Turkey's correction one-way Anova was applied.

***Fam13a* controls NK-cell IFN-γ production**

Different developmental stages of NK cells possess different phenotypic features and effector functions (Hayakawa and Smyth 2006, Fu et al. 2011). Since we observed a significant upregulation in the frequency of the terminally differentiated NK subset, namely, CD27^{-}CD11b^{+}NK cells, we further checked other effector functions of NK cells, including IFN-γ production, one of the most critical roles of NK cells. We expanded NK cells by culturing total splenocytes isolated from *Fam13a* KO and WT littermates in the presence of a high concentration of IL-2 for 5 days **(Fig. 3a)**. We found that *Fam13a* deficiency did not affect the survival and expansion of NK cells *in vitro* (**Fig. 3b, c**). Compared with the *ex vivo* frequency, following IL-2 expansion, the NKG2A^{-}Ly49C/I^{-} and NKG2A^{+}Ly49C/I^{-} subsets still occupied the major portion of the NK cells while the double negative cells represented the most dominant subset (**Fig. 3d, e**). Alike that in the homeostatic condition, the four NK-cell subpopulations based on the combinatory expression of the two major IR NKG2A and Ly49C/I, also presented no obvious difference in the expanded NK cells from *Fam13a* KO or WT mice (**Fig. 3f**). However, when stimulated with the cytokine cocktail including IL-2, IL-12 and IL-15, *Fam13a*-deficient NK cells produced a significantly lower amount of IFN-γ compared with WT counterparts (**Fig. 3g, h**). We further checked the production of IFN-γ among the four NK subsets defined by the combinatory expression of NKG2A and Ly49C/I. In WT mice, among the four subsets the NKG2A^{-}Ly49C/I^{-} cells expressed the lowest amount of IFN-γ while the two NKG2A^{+} subpopulations expressed much higher levels of IFN-γ (**Fig. 3i**). The IFN-γ production of each of the four subpopulations defined by the combination of

NKG2A and Ly49C/I expression was also downregulated in case of *Fam13a* depletion (**Fig. 3j**). Likewise, even when stimulated with the strong-activation cytokine cocktail composed of IL-2, IL-12 and IL-18, *Fam13a*-deficient NK cells still exhibited impaired IFN-γ production capacity (**Fig. 3k, l**). This impairment was mainly reflected in the NKG2A$^-$Ly49C/I$^+$ and NKG2A$^-$Ly49C/I$^-$ subpopulations (**Fig. 3m**). Again similar to that stimulated by the cytokine cocktail with IL-15, the NKG2A$^-$Ly49C/I$^-$ cells expressed the least amount of IFN-γ even in WT NK cells following IL-18 cocktail stimulation (**Fig. 3n**). Taken together, our data demonstrate not only that the two NKG2A$^+$ NK cells produce the highest amount of IFN-γ, representing the best 'educated' ones, but also *Fam13a* depletion impairs IFN-γ production in NK cells under various cytokine-cocktail stimulations *in vitro*.

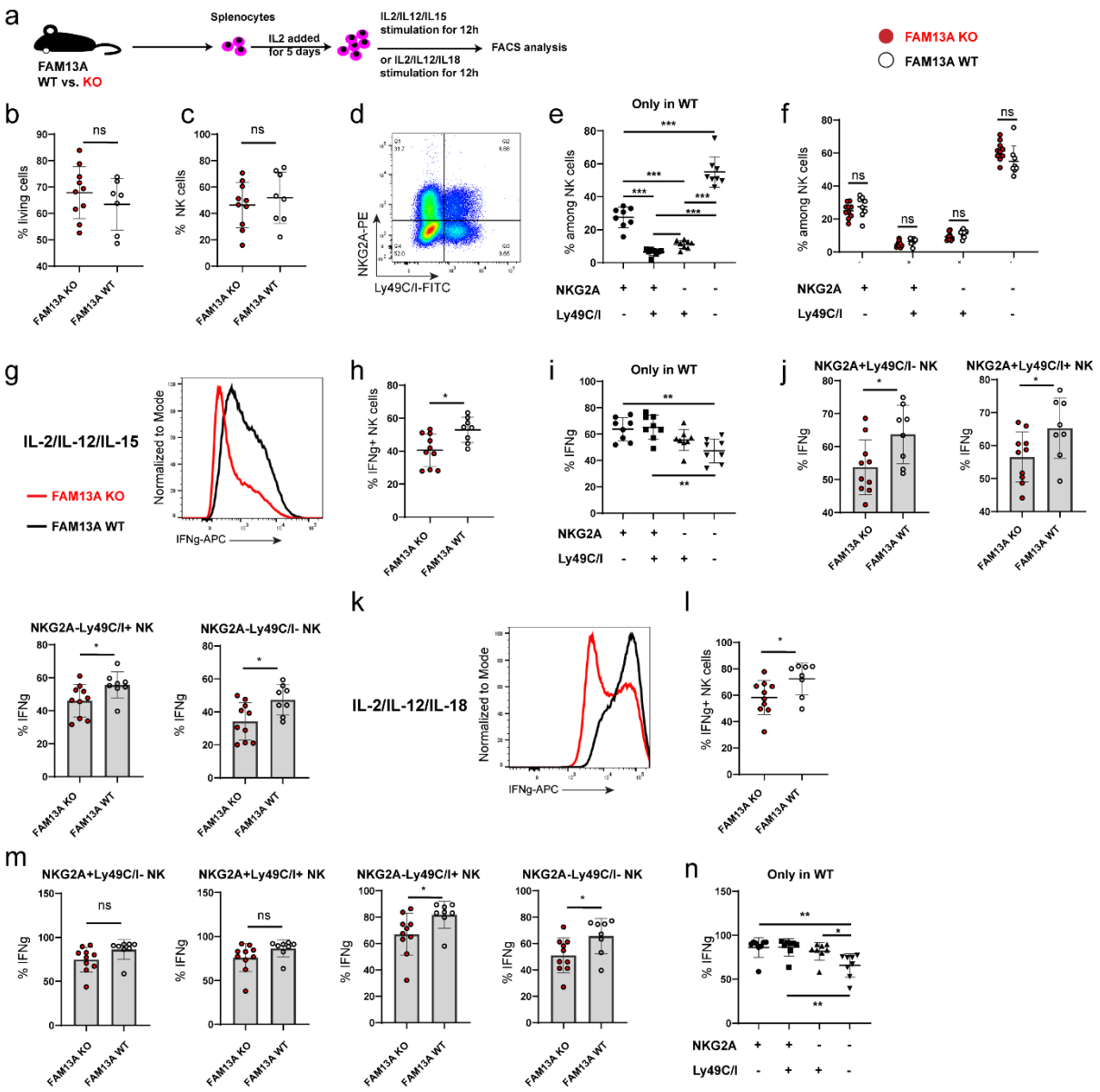

Figure 3. *Fam13a* deficiency impairs NK-cell IFN-γ production

a, Schematic of the experimental setup to stimulate NK cells with cytokine cocktails.

b, c, d, Percentage of living cells (**b**) (KO, n=10; WT, n=7), NK1.1$^+$ NK cells (**c**), NK cell subpopulations based on NKG2A and Ly49C/I expression (**d**) after 5-day expansion in the presence of IL-2 (KO, n=10; WT, n=8).

e, **f**, Percentage of NK cell subpopulations based on NKG2A and Ly49C/I expression after 5-day expansion of splenocytes isolated from WT (**e**) or KO vs. WT mice (**f**) in the presence of IL-2 (KO, n=10; WT, n=8).

g, Representative FACS histogram overlay of IFN-γ production of *Fam13a* KO (red line) and WT (black line) NK cells following 5-day IL-2 expansion and IL-2, IL-12 and IL-15 re-stimulation.

h, Percentage of IFN-γ producing cells among total NK cells after IL-2, IL-12 and IL-15 re-stimulation (KO, n=10; WT, n=8).

i, **j**, Percentage of IFN-γ producing cells among four NK cell subpopulations based on NKG2A and Ly49C/I expression of splenocytes isolated from WT (**i**) or KO vs. WT mice (**j**) (KO, n=10; WT, n=8) after IL-2, IL-12 and IL-15 re-stimulation.

k, Representative FACS histogram overlay of IFN-γ production of *Fam13a* KO (red line) and WT (black line) NK cells after 5-day IL-2 expansion and IL-2, IL-12 and IL-18 re-stimulation.

l, Percentage of IFN-γ producing cells among total NK cells after IL-2, IL-12 and IL-18 re-stimulation.

m, n, Percentage of IFN-γ producing cells among four NK cell subpopulations based on NKG2A and Ly49C/I expression of splenocytes isolated from KO vs. WT (**m**) or WT mice (**n**) after IL-2, IL-12 and IL-18 re-stimulation.

Data are representative of 3 independent experiments. Data are mean± s.d. The p-values are determined by a two-tailed Student's t-test. Results represent three (**b**, **c**, **e**, **f**, **h**, **i, j**, **l, m, n**) independent experiments. n.s. or unlabeled, not significant, *p<=0.05, **p<=0.01 and ***p<=0.001. For subfigure **e, i, n**, Turkey's multiple-comparison correction one-way Anova was applied.

Fam13a modulates NK-cell degranulation and IFN-γ production against tumor cells

To further check the killing capacity of NK cells towards tumour cells, we pre-activated NK cells *in vivo* by injecting the TLR3 agonist Poly (I:C) into *Fam13a* KO and WT littermates (**Fig. 4a**). We then checked the expression of IFN-γ and of the degranulation marker CD107a in NK cells following the incubation with the target tumor cell line YAC-1. CD107a is a degranulation marker of NK cells and CD8$^+$ T cells, which reflects their cytotoxic activity (Alter et al. 2004, Aktas et al. 2009). No clear difference was observed in the percentages of CD107a-expressing cells among total NK cells (**Fig. 4b, c**) and in the absolute number (**Fig. 4d**) of CD107a$^+$ NK cells between *Fam13a* KO and WT mice following Poly (I:C) injection. However, loss of *Fam13a* caused a decreased degranulation capacity per individual NK cell against YAC-1, as indicated by the decreased MFI of CD107a in NK cells (**Fig. 4e**). More precisely, the decrease of CD107a expression was mainly observed in NKG2A$^+$Ly49C/I$^-$ and NKG2A$^-$Ly49C/I$^-$ NK subsets (**Fig. 4f**). Similar to what was observed in IFN-γ production, the degranulation level was lowest also in NKG2A$^-$Ly49C/I$^-$ NK cells, no matter from which genotype

groups (**Fig. 4f, g**). Lower amounts of IFN-γ were produced by *Fam13a* KO NK cells, as shown by the decreased percentage of IFN-γ-expressing NK cells (**Fig. 4h, i**), the decreased absolute number of IFN-γ-expressing NK cells (**Fig. 4j**) and the MFI of IFN-γ per NK cell in IFN-γ $^{+}$ NK cells (**Fig. 4k**). The difference regarding the IFN-γ^{+} population was again mainly found in the two Ly49C/I^{-} subsets, i.e., NKG2A^{+}Ly49C/I^{-} and NKG2A^{-}Ly49C/I^{-} NK cells (**Fig. 4l**). In conclusion, *Fam13a* depletion impairs NK cell degranulation capacity and IFN-γ production.

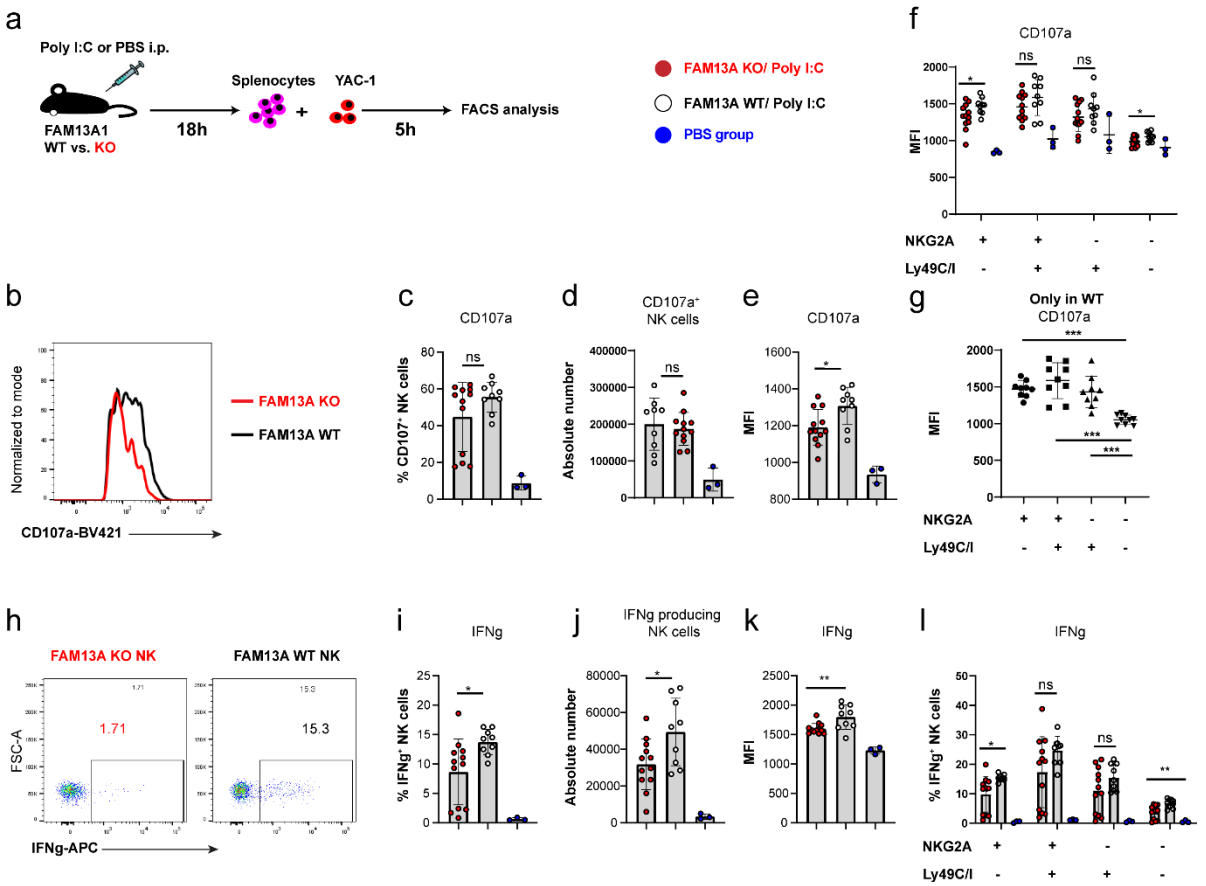

Figure 4. *Fam13a* deficiency leads to impaired NK cell degranulation and IFN-γ secretion against tumor cells after Poly (I:C) activation

a, Schematic of the experimental setup to analyze the degranulation capacity of NK cells. *Fam13a* KO or WT littermates were injected intraperitoneally (i.p.) with 150 µg Poly (I:C) or PBS and then at the next day splenocytes were incubated with YAC-1 cells to evaluate NK cell degranulation and IFN-γ production.

b, Representative FACS histogram overlay of CD107a expression in *Fam13a* KO (red) and WT (black) NK cells against YAC-1 tumor cells.

c, Percentage of CD107a producing NK cells of *Fam13a* KO and WT NK cells against YAC-1 tumor cells (KO, n=12, WT, n=9).

d, Absolute number of CD107a producing NK cells of *Fam13a* KO and WT NK cells against YAC-1 tumor cells (KO, n=12, WT, n=9).

e, Geometric mean (MFI) of CD107a expression intensity in total CD107a$^+$ NK cells of *Fam13a* KO and WT NK cells (KO, n=12, WT, n=9).

f, g, Geometric mean of CD107a expression intensity in CD107a$^+$ NK cell subpopulations based on NKG2A and Ly49C/I expression of of *Fam13a* KO vs. WT NK cells (**f**) or WT NK cells (**g**) (KO, n=12, WT, n=9).

h, Representative FACS plot of IFN-γ expression in gated *Fam13a* KO and WT NK cells against YAC-1 tumor cells.

i, j, Percentage (**i**) and absolute number (**j**) of IFN-γ producing NK cells of *Fam13a* KO and WT NK cells against YAC-1 tumor cells (KO, n=12, WT, n=9).

k, Geometric mean of IFN-γ expression intensity in total IFN-γ$^+$ NK cells of *Fam13a* KO and WT NK cells (KO, n=12, WT, n=9).

l, Percentage of IFN-γ $^+$ NK cells among the four subpopulations based on NKG2A and Ly49C/I expression of *Fam13a* KO and WT NK cells (KO, n=12, WT, n=9). Results represent three (**c**, **d**, **e**, **f**, **g**, **i**, **j**, **k**, **l**) independent experiments. Data are mean ± s.d. The *p*-values are determined by a two-tailed Student's t-test. n.s. or unlabeled, not significant, **p*<=0.05, ***p* <=0.01 and ****p* <=0.001. For subfigure **g**, Turkey's multiple-comparison correction one-way Anova was applied.

Fam13a* deficiency promotes lung metastasis induced by melanoma cells *in vivo

Having shown that *Fam13a* depletion impaired several effector functions of NK cells *in vitro* or *ex vivo*, we sought to further investigate its *in vivo* effects. Since NK cells are critical in the control of metastasis (López-Soto et al. 2017), we induced lung metastasis by transplanting B16F10 melanoma cells. We intravenously injected *Fam13a* KO and WT littermates with B16F10 melanoma cells and evaluated the lung metastases 16 days post inoculation (**Fig. 5a**). Compared with *Fam13a* WT mice, *Fam13a* KO mice had developed much more tumor metastases in the lung (**Fig 5b, c**). Since NK cell-mediated control in melanoma metastasis is critical, we first analysed NK cells in the spleen and lung tissues. The frequency and absolute number of NKp46$^+$NK1.1$^+$ NK cells among CD3$^-$CD19$^-$ splenocytes was much lower in melanoma treated *Fam13a* KO mice compared with those in WT littermates (**Fig. 5d- f**). Likewise, *Fam13a* KO mice also had a lower percentage of infiltrated NKp46$^+$NK1.1$^+$ NK cells among CD3$^-$CD19$^-$ cells in lung in comparison to WT littermates (**Fig. 5g**). Similar to the homeostatic phenotype of *Fam13a* KO NK cells (**Fig. 2d**), a much higher frequency of KLRG1$^+$ cells was also observed among total NK cells in both spleen (**Fig. 5h, i**) and lung (**Fig. 5j**) of *Fam13a* KO mice in comparison with WT littermates. In addition, all the four subpopulations of NK cells based on the expression of the inhibitory receptors NKG2A and Ly49C/I in *Fam13a* KO mice showed a much higher percentage of KLRG1$^+$ cells (**Fig. 5k**). KLRG1 is also regarded as a terminal differentiation marker of

NK cells (Huntington et al. 2007). In the chronic infection model, KLRG1$^+$ NK cells represent an exhausted phenotype and KLRG1 inhibits NK cell IFN-γ production (Wang et al. 2013, Müller-Durovic et al. 2016, Alvarez et al. 2019). This indicates that both the decreased number and dysfunction of NK cells in *Fam13a* KO mice aggravates tumour metastasis and that the dysfunction might be regulated via the enhanced expression of KLRG1.

Since dysregulation of NK cells might also affect T cell-mediated adaptive immunity against tumors, we further checked CD4$^+$ T cells and cytotoxic CD8$^+$ T cells. No big difference was observed for the frequency of CD4$^+$ T cells in spleen between melanoma-treated *Fam13a* KO and WT littermates **(Extended Data Fig. 3a)**. However, we found higher percentages of both FOXP3$^+$ CD4$^+$ Tregs and CD8$^+$ T cells in spleens of *Fam13a* KO mice, the former of which is known to deteriorate tumor progression while the latter of which might ameliorate the tumor development (**Extended Data Fig. 3b, c**). For naïve and memory compartments of T cells, we observed a higher frequency of effector memory (EM) but a lower percentage of naïve CD4$^+$ T cells in *Fam13a* KO mice (**Extended Data Fig. 3d, e**). However, there were significantly higher percentages of PD-1$^+$ CD4$^+$ T cells (**Extended Data Fig. 3f**), indicating more exhausted or activated T cells in *Fam13a* KO mice. Similarly, more EM and central memory (CM) CD8$^+$ T cells as well as PD-1$^+$ CD8$^+$ T cells, although to a lesser extent, but fewer naïve CD8$^+$ T cells were found in *Fam13a* KO mice (**Extended Data Fig. 3g-i**).

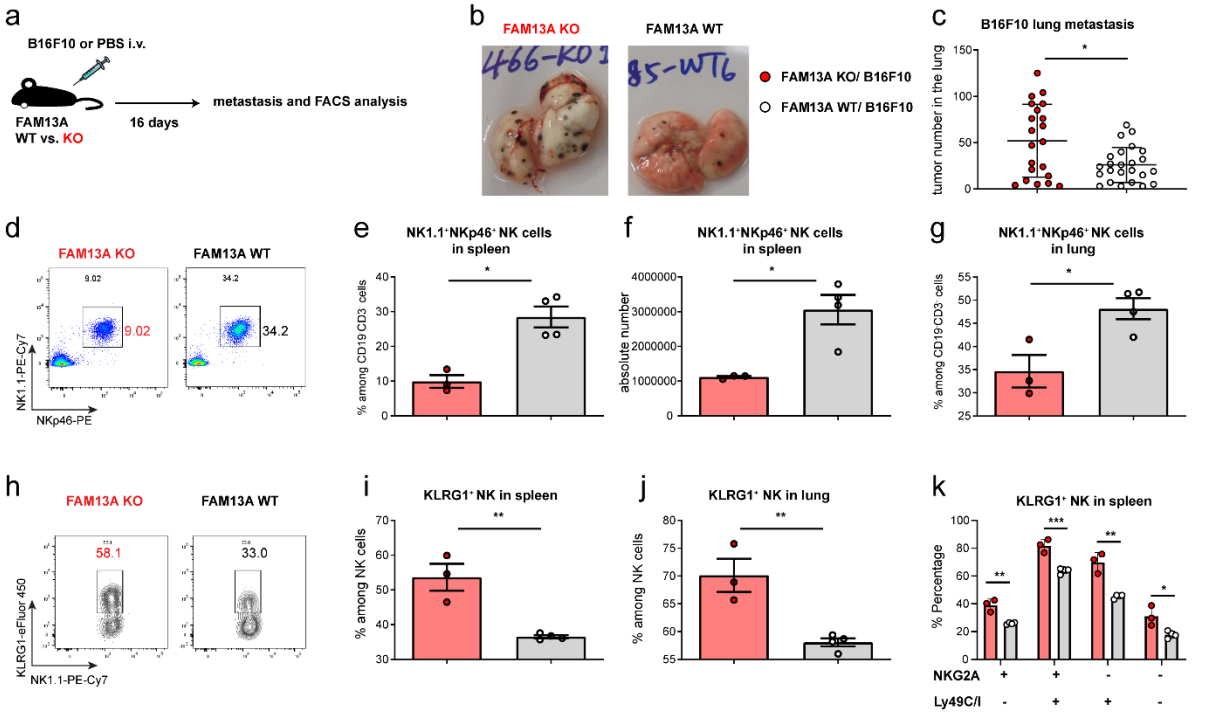

Figure 5. *Fam13a* deficiency dramatically promotes lung metastasis of melanoma cells

a, Schematic of the experimental setup for lung metastasis model induced by B16F10 melanoma cells.

b, c, Representative photographs of freshly isolated lungs (**b**) and quantified metastatic foci (**c**) after B16F10 cell inoculation (pooled KO, n=21; pooled WT, n=24).

d, Representative FACS plot of NKp46 and NK1.1 expression on *Fam13a* KO and WT NK cells.

e, f, Percentage of (**e**) and absolute number (**f**) of NKp46$^+$NK1.1$^+$ NK cells in spleen of *Fam13a* KO and WT littermates (KO, n=3, WT, n=4).

g, Percentage of NKp46$^+$NK1.1$^+$ NK cells in spleen of *Fam13a* KO and WT littermates (KO, n=3, WT, n=4).

h, Representative FACS plot of KLRG1 and NK1.1 expression on *Fam13a* KO and WT NK cells.

i, j, Percentage of KLRG1$^+$ NK cells among total NK cells in spleen (**i**) and lung (**j**) of *Fam13a* KO and WT littermates (KO, n=3, WT, n=4).

k, Percentage of KLRG1$^+$ cells among four NK subpopulations based on NKG2A and Ly49C/I expression in spleen of *Fam13a* KO and WT littermates following B16F10 cell inoculation (KO, n=3, WT, n=4). Results represent two (**e**, **f**, **g**, **i**, **j**, **k**) and four (**c**) independent experiments. Data are mean ± s.d. The *p*-values are determined by a two-tailed Student's t-test. n.s. or unlabeled, not significant, **p*<=0.05, ***p* <=0.01 and ****p* <=0.001. For multiple comparisons, Turkey's correction one-way Anova was applied.

Discussion

In this work, we showed that (i) cytokine-activated NK cells keep a trace of their initial educational profile, and licensing through NKG2A appears as more efficient than that through Ly49C/I, (ii) *Fam13a* inhibits NK cell maturation, as shown through the up-regulation of CD27$^-$CD11b$^+$ cells in the *Fam13A*-

KO animals, (iii) *Fam13a* is required for an optimal NK cell IFN-γ production and degranulation, (iv) *in vivo*, the KO mice develop significantly more lung metastases after intravenous injection of a melanoma cell line, and (v) the absence of *Fam13a* does not seem to have a phenotypic impact on B and T cell numbers and subset distribution, nor on Treg function (at least under homeostasis).

The NK cell education concept is based on the observation that developing NK cells become functional upon recognition of autologous MHC class I molecules *via* specific IR. Several models for education have been proposed (Boudreau and Hsu 2018), such as the licensing model (Kim et al. 2005), the (dis)arming model (Elliott and Yokoyama 2011), the rheostat model (the more specific IR the NK cell expresses, the better educated and more functional the cell is) (Brodin and Hoglund 2008), the *cis-trans* interaction model (IR molecules are engaged with their MHC class I ligand in *cis*, so that the quantity of IR available for *trans* interactions is reduced and the activating threshold of the NK cell decreased) (Zimmer et al. 2001, Doucey et al. 2004, Chalifour et al. 2009). Finally, the confinement model was also proposed, taking into account the adhesion molecules (He and Tian 2017). More recently, from a mechanistic point of view, the presence of dense-core secretory lysosomes containing the cytolytic effector protein granzyme B distinguishes educated from uneducated resting NK cells (Goodridge et al. 2019, Pfefferle et al. 2020).

Previous observations by Kim et al. have revealed that the IR from the Ly49 family can efficiently license NK cells (Kim et al. 2005). Initially neglected, NKG2A was later demonstrated to likewise educate NK cells in mouse and man (Lisovsky et al. 2015, Meyer et al. 2017, Kristensen et al. 2018, Zhang et al. 2019). Our data reveal that the proportion of IFN-γ-producing NKG2A^{+} NK cells (either single positive or associated with Ly49C/I) is significantly higher in both WT mice and *Fam13A-KO* mice than that in Ly49C/I single positive and NKG2A^{-}Ly49C/I^{-} double negative subsets, after a strong cytokine-mediated activation. We chose the cocktail IL-2/IL-12/IL-15 to discriminate potentially differential effects on the four subpopulations. Interleukin-2 alone served as negative, while the cocktail IL-2/IL-12/IL-18 as positive control, as it gives maximal IFN-γ production. An imprint of the initial education profile was still present in a large fraction of the licensed NK cells even after activation, and the expression of NKG2A seemed to confer a higher frequency of IFN-γ-producing cells than the

presence of Ly49C/I. The *Fam13a*-KO NK cells followed the same curve but with significantly lower frequencies of NK cells that accumulated IFN-γ in their cytoplasm. This effect of *Fam13a* was even observable in NK cells strongly activated with IL-2/IL-12/IL-18 on a global level, whereas its influence was only clear among the two NKG2A$^-$ subpopulations. Furthermore, after an *in vivo* pre-activation of NK cells via the TLR3 agonist Poly (I:C), the MFI of CD107a as well as the percentage of IFN-γ$^+$ NK cells followed the same pattern as the education process, which might be less surprising as the cells were harvested after only one night of *in vivo* stimulation. Here again, (i) NKG2A was the most efficient licensing IR, and (ii) the KO NK cells were less functional than the WT mice. Our finding that NKG2A "educates" better than the Ly49 family of IR is somewhat contrasting with the observation of another group (Zhang et al. 2019). In that work, following CRISPR/Cas9-mediated deletion, NKG2A seems to have only a mild effect as opposed to a "moderate" one after the KO of Ly49C and Ly49I, while both groups of IR strongly synergize for an optimal licensing process. However, we observed the most prominent effect of NKG2A after five-day culture in IL-2 and then overnight stimulation with IL-12 and IL-15, whereas Zhang et al. mainly used the Poly (I:C) experimental system. In mice deficient in the CD94 chaperone molecule necessary for the surface expression of the IR NKG2A and the AR NKG2C and NKG2E, no major effects on NK cell functions are observed (Orr et al. 2010), but some doubts exist about the genetic background of those animals (Zhang et al. 2019).

The *Fam13A*-KO animals also displayed a different maturation profile compared to their WT counterparts, as reflected in a much higher frequency of mature CD27$^-$CD11b$^+$ and KLRG1$^+$ NK cells *ex vivo*, which suggests that *Fam13a* has an inhibiting or regulatory effect on NK cell maturation, or preventing to some extent premature entry into the senescent state. As the CD27$^-$CD11b$^+$ NK cells are less proficient in cytokine production and cytotoxic activity than CD27$^+$CD11b$^+$ cells (Hayakawa and Smyth 2006), the simple change in proportion might already explain the functional differences between WT and KO mice, at least in the Poly (I:C) experiments. Furthermore, the extracellular matrix glycoprotein fibronectin is able to selectively keep CD11b$^+$ NK cells viable *in vitro* through a direct interaction with CD11b and with downstream Src and β-catenin, resulting in nuclear translocation of β-catenin and ERK activation (Zhang et al. 2009). Interestingly, β-catenin is inhibited by *Fam13a* (Jiang

et al. 2016), so that in WT mice, a useless accumulation of mature and hypofunctional $CD27^{-}CD11b^{+}$ NK cells might be avoided via this pathway.

Even more striking is the difference between WT and *Fam13a*-KO mice in terms of KLRG1 expression. This is an IR of the C-type lectin superfamily able to inhibit NK cell functions (cytotoxicity and cytokine production) upon recognition of its non-MHC class I ligands, which are E-, N- and R-cadherins (Ito et al. 2006, Banh et al. 2009, Li et al. 2009). The latter are adhesion molecules downregulated on cancer cells. In mice, KLRG1 is expressed on roughly a third of NK cells, but it increases upon infections (Banh et al. 2009, Li et al. 2009). In *Fam13a*-KO mice, particularly in spleen, this value was almost doubled in most of the animals, which might again explain, at least in part, the functional results in the Poly (I:C) stimulation conditions. Importantly, the interaction between KLRG1 and E-cadherin is bidirectional and triggers signaling pathways in both the KLRG1- and the E-cadherin-expressing cells, a process called reverse signaling (Banh et al. 2009). Cadherins are again in turn linked to Wnt/β-catenin, so that one might speculate about the outcome of the interaction for the cadherin-expressing immune cells in *Fam13a*-KO mice, for example macrophages and dendritic cells. On one hand, $cadherin^{+}$ cells would be quite well protected from NK cell-mediated killing. On the other hand, those cells could have increased functional capacities to interact with the adaptive immune system, as *Fam13a* depletion would potentially lead to higher levels of Wnt/β-catenin signaling at least in epithelial cell lines. This hypothesis goes beyond the scope of the present work, but will have to be addressed in future experiments.

In our *in vivo* B16F10 melanoma models, we observed a strong reduction in the number of NK cells in spleen and lung of the KO mice compared to their WT counterparts, but a significantly higher frequency of $KLRG1^{+}$ NK cells. This might suggest at first sight that more NK cells were inhibited, but this would depend on the expression level of the cadherin ligands on the tumor cells. In any case, *Fam13a*-KO mice displayed a significantly higher number of lung metastases compared to the WT animals, which is in accordance with our *in vitro* findings**,** showing a hypofunctional state of KO NK cells. In line with our observation of a higher expression of KLRG1 among NK cells in *Fam13a*-KO mice, KLRG1 neutralization antibody plus anti-PD-1 combinatory treatment vs. the anti-PD-1 therapy alone has

achieved better survival rate and response to tumor volume in B16F10 melanoma models (Greenberg et al. 2019). On the other hand, $CD27^{-}KLRG1^{+}$ NK cells control pulmonary metastasis in the CT26 colon carcinoma model (Renner et al. 2014). Meanwhile, in human studies, a higher expression of KLRG1 was associated with a better survival of the patients with lung adenocarcinoma or skin melanoma (Huntington et al. 2020). According to those two reports, we should have observed fewer metastatic nodules in the KO mice. However, the higher percentage of $KLRG1^{+}$ NK cells in the *Fam13a*-KO mice would be a compensatory factor to better activate the anti-tumor mechanisms in the situation of a decreased number of NK cells, which otherwise would not work as well as in the WT counterparts. More realistically, $KLRG1^{+}$ NK cells possibly produced, as previously described, less IFN-γ than $KLRG1^{-}$ NK cells (Huntington et al. 2007). As we also observed some effects of *Fam13a* on T cells in the induced lung metastasis experiments, further cell-type specific knockout animal models are required to figure out whether our observation is only driven by NK cells or together with other cell types. In short, here we demonstrated a previously unrecognized critical role of *FAM13A* in the maturation and several effector functions of NK cells using both *in vitro* and *in vivo* models. As *FAM13A* is strongly associated with the risk of several common lung diseases, our discovery paves the way to develop a novel potential target to mediate NK cell functions in the fight against complex lung diseases.

Materials and Methods

Mice

Fam13a knock-out (KO) mice [$Fam13a^{tm2a\ (KOMP)Wtsi}$] with C57BL/6N background were obtained from the Knockout Mouse Project (KOMP) Repository at UC Davis. The $Fam13a^{-/-}$ (KO), $Fam13a^{+/-}$ (HET) and $Fam13a^{+/+}$ (WT) mice used in the experiments were age- and gender-matched littermates generated from $Fam13a^{+/-}$ heterozygous breeding pairs. All mice were bred and housed in a specific pathogen-free animal facility. All animal experimental protocols were performed following the approval of the Animal Welfare Structure (AWS) of the University of Luxembourg and the Luxembourg Institute of Health, and in accordance with National and European guidelines about the care and use of laboratory animals.

Flow cytometric analysis of immunophenotype

Cell suspensions were obtained by the mechanical disruption of mouse spleen, peripheral lymph nodes, bone marrow and lung. Red blood cells were then lysed in 1x lysing buffer (555899, BD Bioscience).

One million cells per sample were pre-incubated with purified anti-mouse CD16/CD32 antibody (Fc Block™, 553141, BD Biosciences). Cell surface markers were then stained by part of the following antibodies: anti-mouse CD3-BUV496 (612955, BD Biosciences) (dilution 1:100), anti-mouse CD3-BV421 (562600, BD Biosciences) (dilution 1:100), anti-mouse CD19-BV510 (562956, BD Biosciences) (dilution 1:100), anti-mouse CD19-FITC (11-0193-82, eBioscience) (dilution 1:100), anti-mouse NK1.1-PE-Cy7 (108713, Biolegend) (dilution 1:50), anti-mouse NK1.1-BV421 (562921, BD Bioscience) (dilution 1:100), anti-mouse CD27-FITC (11-0271-82, eBioscience), anti-mouse CD11b-APC (553312, BD Biosciences) (dilution 1:100), anti-mouse CD11b-BUV395 (565976, BD Biosciences) (dilution 1:100), anti-mouse KLRG1-eFluor 450 (48-5893-82, eBioscience) (dilution 1:100), anti-mouse KLRG1-PerCP-Cy5.5 (138417, Biolegend) (dilution 1:100), anti-mouse CD69-PE (553273, BD Biosciences) (dilution 1:200), anti-mouse Ly49C/I-FITC (553276, BD Biosciences) (dilution 1:100), anti-mouse NKG2A-PE (142803, Biolegend) (dilution 1:100), anti-mouse CD69-BV605 (104529, Biolegend) (dilution 1:200), anti-mouse Ly49A-BUV395 (742370, BD Biosciences) (dilution 1:100), anti-mouse Ly49D-BV711 (742559, BD Biosciences) (dilution 1:100), anti-mouse 2B4-FITC (553305, BD Biosciences) (dilution 1:100), anti-mouse Ly49H-BUV395 (744266, BD Biosciences) (dilution 1:100), anti-mouse NKp46-PE (137603, Biolegend) (dilution 1:100), anti-mouse NKG2D-APC (130211, Biolegend) (dilution 1:100), anti-mouse CD4-FITC (11-0042-82, eBioscience) (dilution 1:200), anti-mouse CD8-BUV805 (564920, BD Biosciences) (dilution 1:200), anti-mouse CD25-APC (557192, BD Bioscience) (dilution 1:100), anti-mouse CD44-PE-Cy7 (560569, BD Biosciences) (dilution 1:200), anti-mouse CD62L-PerCP-Cy5.5 (560513, BD Biosciences) (dilution 1:200), anti-mouse PD-1-BV711 (744547, BD Biosciences) (dilution 1:200). Live/dead cells were discriminated by staining cells with the LIVE/DEAD® Fixable Near-IR Dead Cell Stain kit (L10119, Thermo Fisher Scientific) (dilution 1:500). Intracellular staining for Foxp3-APC (126403, Biolegend) (dilution 1:200), Ki-67-BV605 (652413, Biolegend) (dilution 1:200) or Ki-67-eFluor 450 (48-5698-82, eBioscience) (dilution 1:200) was performed by using the Foxp3 Staining Kit (00-5523-00, eBioscience). Of note, all these antibodies might not be necessarily used in one staining panel due to the spectrum compatibility. Samples were measured on a BD LSR Fortessa™ and data were analysed with FlowJo (v10, Tree Star).

Primary murine NK cell in vitro expansion and cytokines activation (NK cell education)

Five million of splenocytes per well in 12-well plate were cultured in 2.5 ml of complete medium with 1000 U/ml of recombinant human (rh) IL-2 (202-IL-010, R&D System) in 37°C, 5% CO2 incubators until day 5. On day 5, the cells were stimulated by 1000 U/ml of rhIL-2 (R&D Systems) and the combination of 10 ng/ml of recombinant murine (rm)IL-12 (210-12, PeproTech Inc) and 40 ng/ml of rmIL-15 (210-15, PeproTech Inc) or 100 ng/ml of rmIL-18 (B004-5, MBL) for one night. Before FACS staining, the cells were incubated with Golgistop (554724, BD Biosciences) (dilution 1:1500) and

Golgiplug (555029, BD Biosciences) (dilution 1:1000) and for 5 hrs. Cell surface markers were stained with anti-mouse CD3-BUV496 (612955, BD Biosciences) (dilution 1:100), anti-mouse NK1.1-PE-CY7 (108713, Biolegend) (dilution 1:50), anti-mouse LY49C/I-FITC (553276, BD Biosciences) (dilution 1:100) and anti-mouse NKG2A-PE (142803, Biolegend) (dilution 1:100). Dead cells were stained by using the LIVE/DEAD® Fixable Near-IR Dead Cell Stain kit (L10119, Thermo Fisher Scientific) (dilution 1:500). For intracellular cytokine staining, cells were first fixed/permeabilized with Cytofix/Cytoperm buffer (554714, BD Biosciences) and then stained with anti-mouse IFN-γ-APC antibody (554413, BD Biosciences) (dilution 1:100) diluted in Perm/Wash buffer (554714, BD Biosciences). NK cell culture medium is the complete DMEM medium (41965039, Thermo Fisher Scientific) with 10% of Fetal Bovine Serum (10500-064, Thermo Fisher Scientific), 100 U/ml Penicillin-Streptomycin (15070-063, Thermo Fisher Scientific), 10 mM HEPES (15630080, Thermo Fisher Scientific) and 55 μM β-mercaptoethanol (M7522, Sigma-Aldrich).

NK cell degranulation assay

Fam13a KO and WT littermates were injected with 150 ug of toxin-free Poly (I:C) (tlrl-pic, InvivoGen) in 100 ul PBS via intraperitoneal injection. Eighteen hours later, the mice were sacrificed and the spleens were harvested. Splenocytes (1 x 10^6) were cultured with 0.5x 10^6 YAC-1 target cells (2:1 ratio) in the presence of anti-mouse CD107a-BV421 antibody (564347, BD Biosciences) (1:100) for 1 hr). Golgiplug and Golgistop were then added for an additional 4-hr incubation. Cells were stained with anti-mouse CD3-BUV496 (612955, BD Biosciences) (dilution 1:100), anti-mouse NK1.1-PE-Cy7 (108713, Biolegend) (dilution 1:50), anti-mouse Ly49C/I-FITC (553276, BD Biosciences) (dilution 1:100), anti-mouse NKG2A-PE (142803, Biolegend) (dilution 1:100) plus Live/dead staining kit (L10119, Thermo Fisher Scientific) (dilution 1:500). Intracellular cytokine IFN-γ were stained as the procedures mentioned above.

Melanoma model for pulmonary metastasis

Fam13a KO and matched *Fam13a* WT littermate mice aged 8 to 10 weeks were used for lung metastasis study following intravenous injection of 2x10^5 B16F10 melanoma cells in 100 µl of PBS. 16 days later, mice were sacrificed. The lung was perfused to remove the excessive blood by slowly injecting cold PBS through the right ventricle. Lung tumor nodules were counted. In addition, the spleens, pLNs and lungs were collected for FACS analysis. For cell isolation from the lung, the organs were cut into small pieces and the tissue digested in the lysis buffer (PBS containing 1.3 mg/ml Collagenase Type II (234155, MERCK), 10% FBS, 50 U/ml Benzonase endonuclease (101654, MERCK), 1mM $MgCl_2$) in a 37°C incubator for 1h. Single cell suspensions for FACS staining were made by filtering of the cells through 40 µM cell strainers (734-2760, VWR).

Real time PCR

Spleen and/or lung were collected from *Fam13a* KO, *Fam13a* Het and *Fam13a* WT mice. NK cells in the spleen were isolated and purified by using mouse NK cell isolation kit II (130-096-892, Miltenyi Biotec). The purity of NK cells was analyzed by FACS. RNA from lung and NK cells of spleen was isolated via using the RNeasy Mini Spin Kit (74104, Qiagen). Genomic DNA was then removed by DNase digestion (79254, Qiagen). The SuperScript III Reverse Transcriptase Kit (18080-044, Invitrogen) was employed for cDNA synthesis. qPCR was performed with the LightCycler 480 SYBR Green I Master Mix (04707516001, Roche Applied Science) as previously described (He et al. 2012, Danileviciute et al. 2019). *Fam13a* mRNA RT-PCR primers are referred according to the literature (Wardhana et al. 2018) (*fwd*: CCG CTG CGA AGC TCA CAG GAA GAT G; *rev*: TTG GTC TCC AGC GTT GCT GAC ATC A). The housekeeping gene for detecting *Fam13a* mRNA expression was *Rps13* in lung and *18s* in splenic NK cells.

Treg suppressive assay

Treg suppressive assay was performed in a way similar to our previous work (Danileviciute et al. 2019). Total T cells from spleen of *Fam13a* KO mice and WT littermates were isolated with CD90.2 microbeads (130-121-278, Miltenyi Biotec). The cells were then stained with the master mix containing LIVE/DEAD® Fixable Near-IR (L10119, Thermo Fisher Scientific) (dilution 1:500), anti-mouse CD25-PE-Cy7 (552880, BD Bioscience) (dilution 1:200) and CD4-FITC (11-0042-82, eBioscience) (dilution 1:200) antibodies at 4 °C for 30 min. After staining, Tregs ($CD4^{+}CD25^{high}$) and conventional $CD4^{+}CD25^{-}$ T cells (Tconv) were sorted by BD FACSAria™ III sorter. Tconv cells from WT mice were labelled with a final concentration of 1 µM CellTrace™ CFSE (C34554, Life Technology). Splenocytes depleted of T cells were used as antigen-presenting cells (APCs)/feeder cells and were irradiated in RS2000 (Rad Source Technologies) with a total dose of 30 Gy within a period of 10 mins. $1x10^5$ Tconv cells and Treg cells were co-cultured at different ratios in the presence of $2x10^5$ irradiated APCs and 1 µg/ml soluble anti-CD3 antibody (554829, BD Biosciences). The cells were cultured in T-cell complete media which consists of RPMI 1640 medium (21870084, Thermo Fisher Scientific) supplemented with 50 U/ml penicillin, 10 mM HEPES (15630080, Thermo Fisher Scientific), 10% heat-inactivated fetal bovine serum (FBS) (10500-064, Thermo Fisher Scientific), 50 µg streptomycin (15070-063, Thermo Fisher Scientific), 2 mM GlutaMAX (35050061,Thermo Fisher Scientific), 1 mM sodium pyruvate (11360070, Thermo Fisher Scientific), 0.1 mM non-essential amino acids (M7145, Sigma Aldrich) and 50 µM beta-mercaptoethanol (M7522, Sigma Aldrich) at 37°C, 5% CO_2 incubator. The proliferation of Tconv cells labeled by CFSE was measured after three-day co-culturing using a BD LSR Fortessa™.

Statistical analysis

P-values were calculated by Graphpad Prism software with non-paired two-tailed Student t test as presented in the corresponding figure legends. If multiple comparison to be considered, we applied Turkey's correction one-way Anova. P-values under 0.05 were considered as statistically significant (*p

< 0.05, **p < 0.01, ***p < 0.001; n.s. or non-labelled between the compared groups, not significant). Data were presented as mean ± s.d.

Acknowledgements

F.Q.H. and the lab was partially supported by Luxembourg National Research Fund (FNR) CORE programme grant (CORE/14/BM/8231540/GeDES), FNR AFR-RIKEN bilateral programme (TregBAR, F.Q.H. and M.O.), PRIDE programme grants (PRIDE/11012546/NEXTIMMUNE and PRIDE/10907093/CRITICS). N.Z., C.C. and N.P. were supported through FNR AFR PhD programme (PHD-2015-1/9989160, PRIDE/10907093/CRITICS and PRIDE/11012546/NEXTIMMUNE, respectively). The work was also partially supported through intramural funding of LIH and LCSB through Ministry of Higher Education and Research (MESR) of Luxembourg.

Author contributions

N.Z. performed major part of the experimental work, data analyses and drafted the manuscript. M.T., C.C., N.P., C.M., C.D., A.B., D.G., X.D., A.P. and C.L. performed different cellular or mice work. R.B., M.O., J.Z., and F.Q.H. provided substantial insights and supervision into the project. F.Q.H. and J.Z. oversaw the whole project and revised the manuscript. F.Q.H. conceived the project.

Declaration of interests

The authors declare no competing interests.

Supplementary information

Supplementary or extended data figures are directly attached in the end.

Extended Data Figures

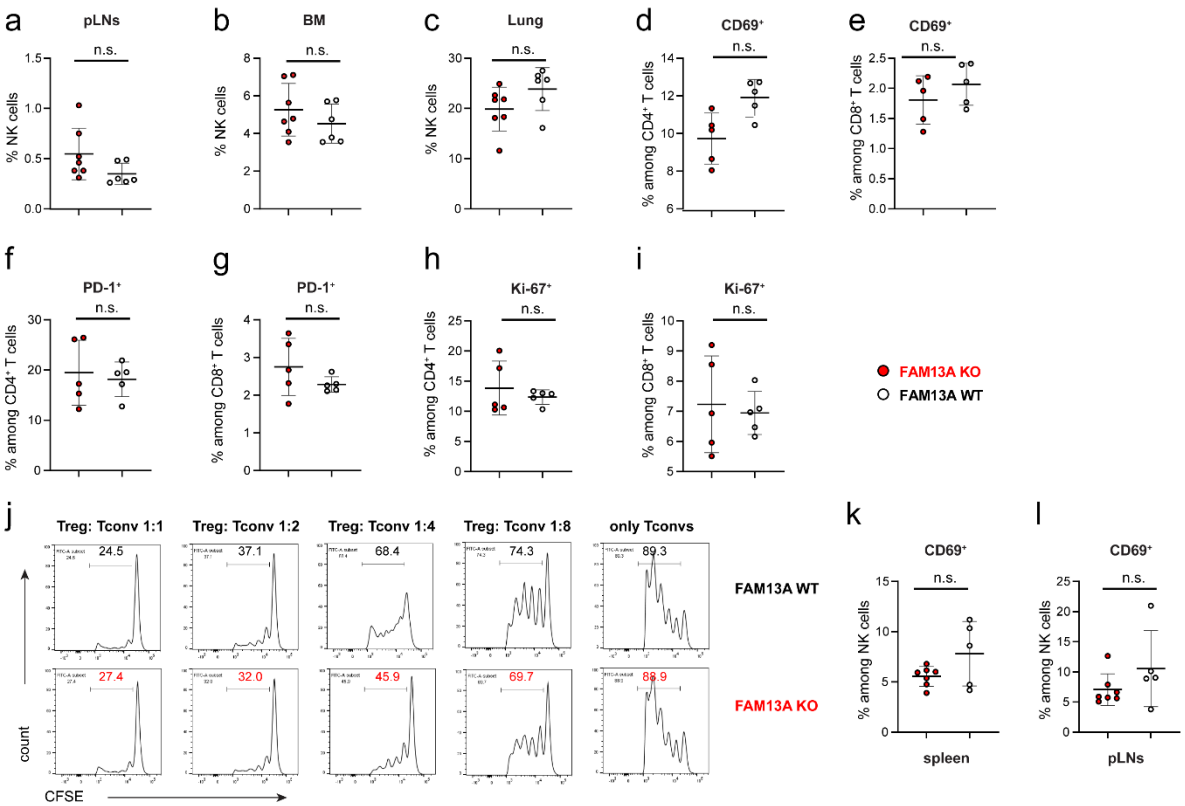

Extended Data Figure 1. Extended immunophenotyping analysis of *Fam13a* KO vs. WT mice

a, b, c, Percentages of NK cells in peripheral lymph nodes (pLNs) (**a**, KO, n=7; WT, n=6), bone marrow (BM) (**b**, KO, n=7; WT, n=6) and lung (**c**, KO, n=7; WT, n=6) of *Fam13a* KO and WT littermates.

d, e, Percentages of CD69$^+$ CD4$^+$ T cells among total CD4$^+$ T cells (**d**, KO, n= 5; WT, n=5) and CD69$^+$CD8$^+$ T cells among total CD8$^+$ T cells (**e**) in spleen of *Fam13a* KO and WT littermates.

f, g, Percentages of PD-1$^+$ CD4$^+$ T cells among total CD4$^+$ T cells (**h**, KO, n= 5; WT, n=5) and PD-1$^+$CD8$^+$ T cells among total CD8$^+$ T cells (**i**) in spleen of *Fam13a* KO and WT littermates.

h, i, Percentages of Ki-67$^+$ CD4$^+$ T cells among total CD$^+$ T cells (**j**, KO, n= 5; WT, n=5) and Ki-67$^+$CD8$^+$ T cells among total CD8$^+$ T cells (**k**) in spleen of *Fam13a* KO and WT littermates.

j, *In-vitro* suppression assay of *Fam13a* KO or WT Tregs in co-culture with Tconv cells at different ratios and irradiated feeder cells in the presence of anti-CD3 antibody for 3 days. Enlarged number in each histogram represents percentage of dividing cells from the total living Tconv population.

k, l, Percentages of CD69$^+$NK cells in spleen (**k**, KO, n= 7; WT, n=5) and peripheral lymph nodes (pLNs) (**l**, KO, n=7; WT, n=6) of *Fam13a* KO and WT littermates. Results represent three (**a, b**, **c**, **k**, **l**) and four (**d**, **e**, **f**, **g**, **h**, **i**, **j**) independent experiments. Data are mean ± s.d. The *p*-values are determined by a two-tailed Student's t-test. n.s. or unlabeled, not significant, **p*<=0.05, ***p* <=0.01 and ****p* <=0.001.

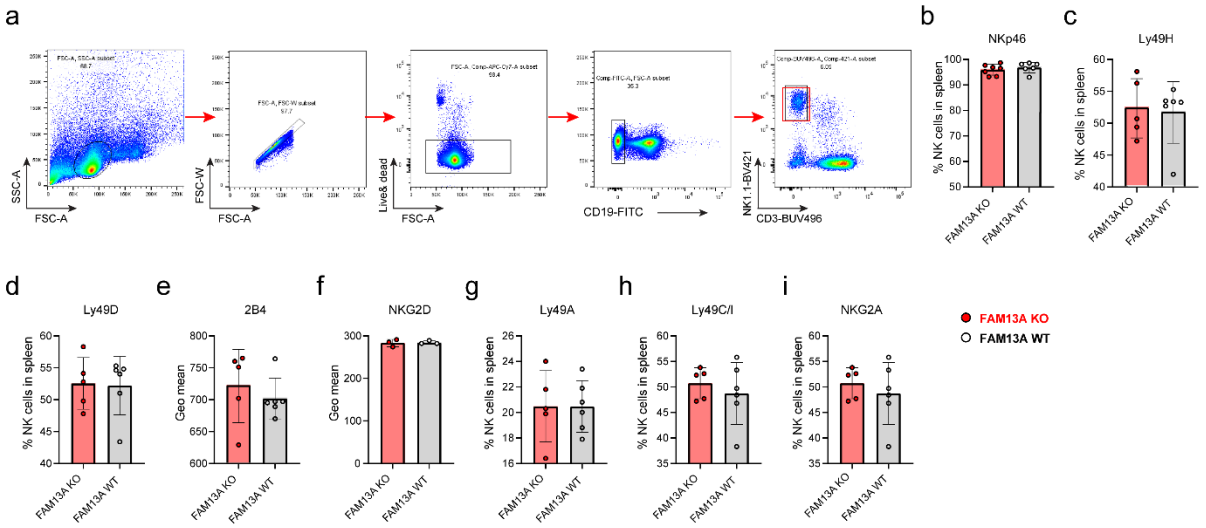

Extended Data Figure 2. Extended analysis of NK-cell activating and inhibitory receptors of *Fam13a* KO mice vs. WT mice

a, Representative FACS gating strategy of NK cells from splenocyte singlets stained with live and dead staining dye, anti-CD19, anti-CD3 and anti-NK1.1 antibodies.

b, c, d, Percentages of NK cells expressing activating receptors NKp46 (**b**), Ly49H (**c**) and Ly49D (**d**) among *Fam13a* KO and WT littermates (KO, n=5; WT, n=6).

e, f, Geometric mean of 2B4 and NKG2D expression in *Fam13a* KO and WT NK cells.

g, h, i, Percentages of NK cells expression inhibitory receptors Ly49A (**g**), Ly49C/I (**h**) and NKG2A (**i**) among *Fam13a* KO and WT littermates (KO, n=5; WT, n=6).

Results represent three (**b-i**) independent experiments. Data are mean± s.d. The p-values are determined by a two-tailed Student's t-test. n.s. or unlabeled, not significant, *p<=0.05, **p<=0.01 and ***p<=0.001.

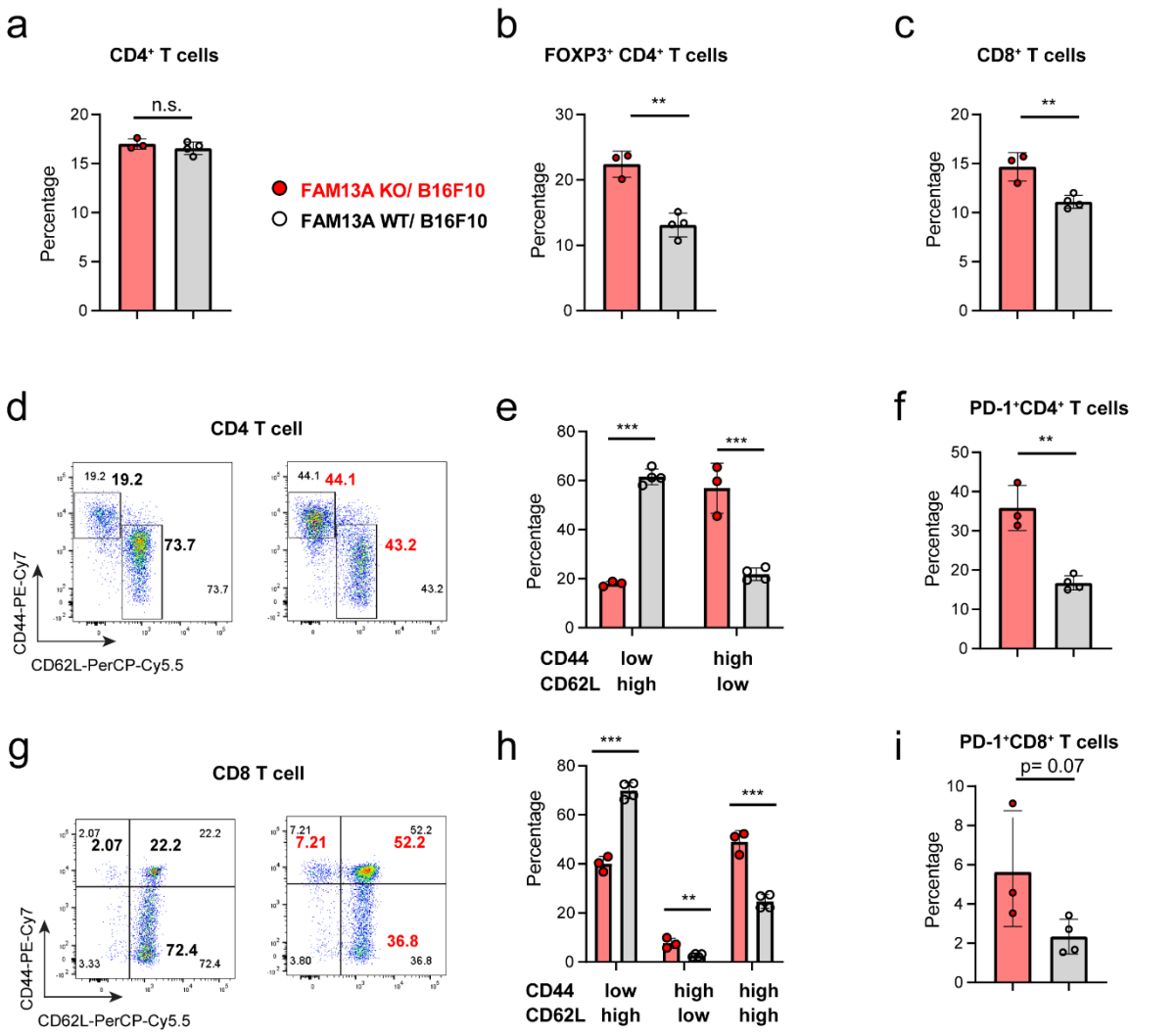

Extended Data Figure 3. Extended analysis of immune cells in the B16F10-melanoma lung metastasis model

a, b, c, Frequency of CD4$^+$ T cells (**d**), FOXP3$^+$CD4$^+$ T cells (**e**) and CD8$^+$ T cells (**f**) in spleen of *Fam13a* KO and WT littermates (KO, n=3, WT, n=4).

d, Representative FACS plot of naïve (CD62L^{hi} CD44^{low}) and effector memory (EM) (CD62L^{low} CD44^{hi} CD4$^+$ T cells in spleen of *Fam13a* KO and WT littermates.

e, f, Percentage of naïve, EM (**e**) and PD-1$^+$ (**f**) among CD4$^+$ T cells in spleen of *Fam13a* KO and WT littermates(KO, n=3, WT, n=4).

g, Representative FACS plot of naïve (CD62L^{hi} CD44^{low}) and effector memory (EM) (CD62L^{low} CD44^{hi} CD8$^+$ T cells in spleen of *Fam13a* KO and WT littermates.

h, i, Percentage of naïve, EM (**h**) and PD-1$^+$ (**i**) among CD8$^+$ T cells in spleen of *Fam13a* KO and WT littermates (KO, n=3, WT, n=4).

Results represent two (**a-c**, **e**, **f**, **h**, **i**) independent experiments. Data are mean ± s.d. The *p*-values are determined by a two-tailed Student's t-test. n.s. or unlabeled, not significant, **p*<=0.05, ***p* <=0.01 and ****p* <=0.001. For multiple comparisons, Turkey's correction one-way Anova was applied.

References

Aktas, E., Kucuksezer, U. C., Bilgic, S., Erten, G. and Deniz, G. (2009). "Relationship between CD107a expression and cytotoxic activity." Cellular immunology **254**(2): 149-154.

Al Omar, S. Y., Marshall, E., Middleton, D. and Christmas, S. E. (2011). "Increased killer immunoglobulin-like receptor expression and functional defects in natural killer cells in lung cancer." Immunology **133**(1): 94-104.

Alter, G., Malenfant, J. M. and Altfeld, M. (2004). "CD107a as a functional marker for the identification of natural killer cell activity." Journal of immunological methods **294**(1-2): 15-22.

Alvarez, M., Simonetta, F., Baker, J., Pierini, A., Wenokur, A. S., Morrison, A. R., Murphy, W. J. and Negrin, R. S. (2019). "Regulation of murine NK cell exhaustion through the activation of the DNA damage repair pathway." JCI insight **4**(14).

Banh, C., Fugere, C. and Brossay, L. (2009). "Immunoregulatory functions of KLRG1 cadherin interactions are dependent on forward and reverse signaling." Blood **114**(26): 5299-5306.

Boudreau, J. E. and Hsu, K. C. (2018). "Natural Killer Cell Education and the Response to Infection and Cancer Therapy: Stay Tuned." Trends Immunol **39**(3): 222-239.

Brodin, P. and Hoglund, P. (2008). "Beyond licensing and disarming: a quantitative view on NK-cell education." Eur J Immunol **38**(11): 2934-2937.

Caligiuri, M. A. (2008). "Human natural killer cells." Blood **112**(3): 461-469.

Castaldi, P. J., Guo, F., Qiao, D., Du, F., Naing, Z. Z. C., Li, Y., Pham, B., Mikkelsen, T. S., Cho, M. H., Silverman, E. K. and Zhou, X. (2019). "Identification of Functional Variants in the FAM13A Chronic Obstructive Pulmonary Disease Genome-Wide Association Study Locus by Massively Parallel Reporter Assays." Am J Respir Crit Care Med **199**(1): 52-61.

Cerwenka, A. and Lanier, L. L. (2016). "Natural killer cell memory in infection, inflammation and cancer." Nat Rev Immunol **16**(2): 112-123.

Chalifour, A., Scarpellino, L., Back, J., Brodin, P., Devevre, E., Gros, F., Levy, F., Leclercq, G., Hoglund, P., Beermann, F. and Held, W. (2009). "A Role for cis Interaction between the Inhibitory Ly49A receptor and MHC class I for natural killer cell education." Immunity **30**(3): 337-347.

Chiossone, L., Chaix, J., Fuseri, N., Roth, C., Vivier, E. and Walzer, T. (2009). "Maturation of mouse NK cells is a 4-stage developmental program." Blood **113**(22): 5488-5496.

Cho, M. H., Boutaoui, N., Klanderman, B. J., Sylvia, J. S., Ziniti, J. P., Hersh, C. P., DeMeo, D. L., Hunninghake, G. M., Litonjua, A. A., Sparrow, D., Lange, C., Won, S., Murphy, J. R., Beaty, T. H., Regan, E. A., Make, B. J., Hokanson, J. E., Crapo, J. D., Kong, X., Anderson, W. H., Tal-Singer, R., Lomas, D. A., Bakke, P., Gulsvik, A., Pillai, S. G. and Silverman, E. K. (2010). "Variants in FAM13A are associated with chronic obstructive pulmonary disease." Nat Genet **42**(3): 200-202.

Cong, J. and Wei, H. (2019). "Natural Killer Cells in the Lungs." Front Immunol **10**: 1416.

Corvol, H., Rousselet, N., Thompson, K. E., Berdah, L., Cottin, G., Foussigniere, T., Longchampt, E., Fiette, L., Sage, E., Prunier, C., Drumm, M., Hodges, C. A., Boëlle, P. Y. and Guillot, L. (2018). "FAM13A is a modifier gene of cystic fibrosis lung phenotype regulating rhoa activity, actin cytoskeleton dynamics and epithelial-mesenchymal transition." J Cyst Fibros **17**(2): 190-203.

Danileviciute, E., Zeng, N., Capelle, C., Paczia, N., Gillespie, M. A., Kurniawan, H., Coowar, D., Vogt Weisenhorn, D. M., Giro, G. G., Grusdat, M., Baron, A., Guerin, C., Franchina, D. G., Léonard, C., Domingues, O., Delhalle, S., Wurst, W., Schwamborn, J. C., Krüger, R., Ranish, J., Brenner, D., Linster,

C. L., Balling, R., Ollert, M. and He, F. Q. (2019). "PARK7/DJ-1 promotes pyruvate dehydrogenase activity and maintains Treg homeostasis." bioRxiv: 2019.2012.2020.884809.

Demaria, O., Cornen, S., Daeron, M., Morel, Y., Medzhitov, R. and Vivier, E. (2019). "Harnessing innate immunity in cancer therapy." Nature **574**(7776): 45-56.

Doucey, M. A., Scarpellino, L., Zimmer, J., Guillaume, P., Luescher, I. F., Bron, C. and Held, W. (2004). "Cis association of Ly49A with MHC class I restricts natural killer cell inhibition." Nat Immunol **5**(3): 328-336.

Eisenhut, F., Heim, L., Trump, S., Mittler, S., Sopel, N., Andreev, K., Ferrazzi, F., Ekici, A. B., Rieker, R., Springel, R., Assmann, V. L., Lechmann, M., Koch, S., Engelhardt, M., Warnecke, C., Trufa, D. I., Sirbu, H., Hartmann, A. and Finotto, S. (2017). "FAM13A is associated with non-small cell lung cancer (NSCLC) progression and controls tumor cell proliferation and survival." Oncoimmunology **6**(1): e1256526.

Elliott, J. M. and Yokoyama, W. M. (2011). "Unifying concepts of MHC-dependent natural killer cell education." Trends Immunol **32**(8): 364-372.

Elpek, K. G., Rubinstein, M. P., Bellemare-Pelletier, A., Goldrath, A. W. and Turley, S. J. (2010). "Mature natural killer cells with phenotypic and functional alterations accumulate upon sustained stimulation with IL-15/IL-15Ralpha complexes." Proceedings of the National Academy of Sciences of the United States of America **107**(50): 21647-21652.

Eriksson Strom, J., Pourazar, J., Linder, R., Blomberg, A., Lindberg, A., Bucht, A. and Behndig, A. F. (2018). "Cytotoxic lymphocytes in COPD airways: increased NK cells associated with disease, iNKT and NKT-like cells with current smoking." Respir Res **19**(1): 244.

Fu, B., Wang, F., Sun, R., Ling, B., Tian, Z. and Wei, H. (2011). "CD11b and CD27 reflect distinct population and functional specialization in human natural killer cells." Immunology **133**(3): 350.

Goodridge, J. P., Jacobs, B., Saetersmoen, M. L., Clement, D., Hammer, Q., Clancy, T., Skarpen, E., Brech, A., Landskron, J., Grimm, C., Pfefferle, A., Meza-Zepeda, L., Lorenz, S., Wiiger, M. T., Louch, W. E., Ask, E. H., Liu, L. L., Oei, V. Y. S., Kjallquist, U., Linnarsson, S., Patel, S., Tasken, K., Stenmark, H. and Malmberg, K. J. (2019). "Remodeling of secretory lysosomes during education tunes functional potential in NK cells." Nat Commun **10**(1): 514.

Greenberg, S. A., Kong, S. W., Thompson, E. and Gulla, S. V. (2019). "Co-inhibitory T cell receptor KLRG1: human cancer expression and efficacy of neutralization in murine cancer models." Oncotarget **10**(14): 1399-1406.

Guo, Y., Lin, H., Gao, K., Xu, H., Deng, X., Zhang, Q., Luo, Z., Sun, S. and Deng, H. (2011). "Genetic analysis of IREB2, FAM13A and XRCC5 variants in Chinese Han patients with chronic obstructive pulmonary disease." Biochemical and biophysical research communications **415**(2): 284-287.

Hayakawa, Y. and Smyth, M. J. (2006). "CD27 dissects mature NK cells into two subsets with distinct responsiveness and migratory capacity." The Journal of Immunology **176**(3): 1517-1524.

He, F., Chen, H., Probst-Kepper, M., Geffers, R., Eifes, S., Del Sol, A., Schughart, K., Zeng, A. P. and Balling, R. (2012). "PLAU inferred from a correlation network is critical for suppressor function of regulatory T cells." Mol Syst Biol **8**: 624.

He, Y. and Tian, Z. (2017). "NK cell education via nonclassical MHC and non-MHC ligands." Cell Mol Immunol **14**(4): 321-330.

Hervier, B., Russick, J., Cremer, I. and Vieillard, V. (2019). "NK Cells in the Human Lungs." Front Immunol **10**: 1263.

Hirano, C., Ohshimo, S., Horimasu, Y., Iwamoto, H., Fujitaka, K., Hamada, H., Hattori, N., Shime, N., Bonella, F., Guzman, J., Costabel, U. and Kohno, N. (2017). "FAM13A polymorphism as a prognostic factor in patients with idiopathic pulmonary fibrosis." Respir Med **123**: 105-109.

Höglund, P. and Brodin, P. (2010). "Current perspectives of natural killer cell education by MHC class I molecules." Nature Reviews Immunology **10**(10): 724.

Huntington, N. D., Cursons, J. and Rautela, J. (2020). "The cancer-natural killer cell immunity cycle." Nat Rev Cancer **20**(8): 437-454.

Huntington, N. D., Tabarias, H., Fairfax, K., Brady, J., Hayakawa, Y., Degli-Esposti, M. A., Smyth, M. J., Tarlinton, D. M. and Nutt, S. L. (2007). "NK cell maturation and peripheral homeostasis is associated with KLRG1 up-regulation." J Immunol **178**(8): 4764-4770.

Huntington, N. D., Tabarias, H., Fairfax, K., Brady, J., Hayakawa, Y., Degli-Esposti, M. A., Smyth, M. J., Tarlinton, D. M. and Nutt, S. L. (2007). "NK cell maturation and peripheral homeostasis is associated with KLRG1 up-regulation." the Journal of Immunology **178**(8): 4764-4770.

Ito, M., Maruyama, T., Saito, N., Koganei, S., Yamamoto, K. and Matsumoto, N. (2006). "Killer cell lectin-like receptor G1 binds three members of the classical cadherin family to inhibit NK cell cytotoxicity." J Exp Med **203**(2): 289-295.

Janssen, L. M., Ramsay, E. E., Logsdon, C. D. and Overwijk, W. W. (2017). "The immune system in cancer metastasis: friend or foe?" Journal for immunotherapy of cancer **5**(1): 79.

Jiang, Z., Lao, T., Qiu, W., Polverino, F., Gupta, K., Guo, F., Mancini, J. D., Naing, Z. Z. C., Cho, M. H. and Castaldi, P. J. (2016). "A chronic obstructive pulmonary disease susceptibility gene, FAM13A, regulates protein stability of β-catenin." American journal of respiratory and critical care medicine **194**(2): 185-197.

Kim, S., Kim, H., Cho, N., Lee, S. K., Han, B. G., Sull, J. W., Jee, S. H. and Shin, C. (2015). "Identification of FAM13A gene associated with the ratio of FEV1 to FVC in Korean population by genome-wide association studies including gene-environment interactions." J Hum Genet **60**(3): 139-145.

Kim, S., Poursine-Laurent, J., Truscott, S. M., Lybarger, L., Song, Y. J., Yang, L., French, A. R., Sunwoo, J. B., Lemieux, S., Hansen, T. H. and Yokoyama, W. M. (2005). "Licensing of natural killer cells by host major histocompatibility complex class I molecules." Nature **436**(7051): 709-713.

Kristensen, A. B., Kent, S. J. and Parsons, M. S. (2018). "Contribution of NK Cell Education to both Direct and Anti-HIV-1 Antibody-Dependent NK Cell Functions." J Virol **92**(11).

Kusnierczyk, P. (2013). "Killer cell immunoglobulin-like receptor gene associations with autoimmune and allergic diseases, recurrent spontaneous abortion, and neoplasms." Front Immunol **4**: 8.

Li, Y., Hofmann, M., Wang, Q., Teng, L., Chlewicki, L. K., Pircher, H. and Mariuzza, R. A. (2009). "Structure of natural killer cell receptor KLRG1 bound to E-cadherin reveals basis for MHC-independent missing self recognition." Immunity **31**(1): 35-46.

Lisovsky, I., Isitman, G., Song, R., DaFonseca, S., Tremblay-McLean, A., Lebouche, B., Routy, J. P., Bruneau, J. and Bernard, N. F. (2015). "A Higher Frequency of NKG2A+ than of NKG2A- NK Cells Responds to Autologous HIV-Infected CD4 Cells irrespective of Whether or Not They Coexpress KIR3DL1." J Virol **89**(19): 9909-9919.

López-Soto, A., Gonzalez, S., Smyth, M. J. and Galluzzi, L. (2017). "Control of Metastasis by NK Cells." Cancer Cell **32**(2): 135-154.

Meyer, C. E., Key, P. N., Zhu, T., Shabsovich, M., Ni, A. and Tripathy, S. K. (2017). "Expression of the inhibitory receptor NKG2A correlates with increased liver and splenic NK cell response to activating receptor engagement." Immun Inflamm Dis **5**(2): 177-189.

Müller-Durovic, B., Lanna, A., Covre, L. P., Mills, R. S., Henson, S. M. and Akbar, A. N. (2016). "Killer Cell Lectin-like Receptor G1 Inhibits NK Cell Function through Activation of Adenosine 5′-Monophosphate–Activated Protein Kinase." The Journal of Immunology **197**(7): 2891-2899.

Orr, M. T., Wu, J., Fang, M., Sigal, L. J., Spee, P., Egebjerg, T., Dissen, E., Fossum, S., Phillips, J. H. and Lanier, L. L. (2010). "Development and function of CD94-deficient natural killer cells." PLoS One **5**(12): e15184.

Pascual-Guardia, S., Ataya, M., Ramirez-Martinez, I., Yelamos, J., Chalela, R., Bellido, S., Lopez-Botet, M. and Gea, J. (2020). "Adaptive NKG2C+ natural killer cells are related to exacerbations and nutritional abnormalities in COPD patients." Respir Res **21**(1): 63.

Pfefferle, A., Jacobs, B., Haroun-Izquierdo, A., Kveberg, L., Sohlberg, E. and Malmberg, K. J. (2020). "Deciphering Natural Killer Cell Homeostasis." Front Immunol **11**: 812.

Platonova, S., Cherfils-Vicini, J., Damotte, D., Crozet, L., Vieillard, V., Validire, P., Andre, P., Dieu-Nosjean, M. C., Alifano, M., Regnard, J. F., Fridman, W. H., Sautes-Fridman, C. and Cremer, I. (2011). "Profound coordinated alterations of intratumoral NK cell phenotype and function in lung carcinoma." Cancer Res **71**(16): 5412-5422.

Renner, P., Rovira, J., Klein, C., Schlitt, H. J., Geissler, E. K. and Kroemer, A. (2014). "KLRG1(+) natural killer cells protect against pulmonary metastatic disease by immunosurveillance." Oncoimmunology **3**: e28328.

Schmiedel, B. J., Singh, D., Madrigal, A., Valdovino-Gonzalez, A. G., White, B. M., Zapardiel-Gonzalo, J., Ha, B., Altay, G., Greenbaum, J. A., McVicker, G., Seumois, G., Rao, A., Kronenberg, M., Peters, B. and Vijayanand, P. (2018). "Impact of Genetic Polymorphisms on Human Immune Cell Gene Expression." Cell **175**(6): 1701-1715 e1716.

van der Plaat, D. A., de Jong, K., Lahousse, L., Faiz, A., Vonk, J. M., van Diemen, C. C., Nedeljkovic, I., Amin, N., Brusselle, G. G., Hofman, A., Brandsma, C. A., Bossé, Y., Sin, D. D., Nickle, D. C., van Duijn, C. M., Postma, D. S. and Boezen, H. M. (2017). "Genome-wide association study on the FEV(1)/FVC ratio in never-smokers identifies HHIP and FAM13A." J Allergy Clin Immunol **139**(2): 533-540.

Vesely, M. D., Kershaw, M. H., Schreiber, R. D. and Smyth, M. J. (2011). "Natural innate and adaptive immunity to cancer." Annual review of immunology **29**: 235-271.

Wang, B., Liang, B., Yang, J., Xiao, J., Ma, C., Xu, S., Lei, J., Xu, X., Liao, Z., Liu, H., Ou, X. and Feng, Y. (2013). "Association of FAM13A polymorphisms with COPD and COPD-related phenotypes in Han Chinese." Clin Biochem **46**(16-17): 1683-1688.

Wang, J. M., Cheng, Y. Q., Shi, L., Ying, R. S., Wu, X. Y., Li, G. Y., Moorman, J. P. and Yao, Z. Q. (2013). "KLRG1 negatively regulates natural killer cell functions through the Akt pathway in individuals with chronic hepatitis C virus infection." Journal of virology **87**(21): 11626-11636.

Wardhana, D. A., Ikeda, K., Barinda, A. J., Nugroho, D. B., Qurania, K. R., Yagi, K., Miyata, K., Oike, Y., Hirata, K.-i. and Emoto, N. (2018). "Family with sequence similarity 13, member A modulates adipocyte insulin signaling and preserves systemic metabolic homeostasis." Proceedings of the National Academy of Sciences **115**(7): 1529-1534.

Yao, M. Y., Zhang, W. H., Ma, W. T., Liu, Q. H., Xing, L. H. and Zhao, G. F. (2019). "microRNA-328 in exosomes derived from M2 macrophages exerts a promotive effect on the progression of pulmonary fibrosis via FAM13A in a rat model." Exp Mol Med **51**(6): 1-16.

Young, R. P., Hopkins, R. J., Hay, B. A., Whittington, C. F., Epton, M. J. and Gamble, G. D. (2011). "FAM13A locus in COPD is independently associated with lung cancer–evidence of a molecular genetic link between COPD and lung cancer." The application of clinical genetics **4**: 1.

Yu, Y., Mao, L., Lu, X., Yuan, W., Chen, Y., Jiang, L., Ding, L., Sang, L., Xu, Z. and Tian, T. (2019). "Functional Variant in 3′ UTR of FAM13A Is Potentially Associated with Susceptibility and Survival of Lung Squamous Carcinoma." DNA and cell biology **38**(11): 1269-1277.

Zhang, T., Liu, S., Yang, P., Han, C., Wang, J., Liu, J., Han, Y., Yu, Y. and Cao, X. (2009). "Fibronectin maintains survival of mouse natural killer (NK) cells via CD11b/Src/beta-catenin pathway." Blood **114**(19): 4081-4088.

Zhang, X., Feng, J., Chen, S., Yang, H. and Dong, Z. (2019). "Synergized regulation of NK cell education by NKG2A and specific Ly49 family members." Nat Commun **10**(1): 5010.

Zhang, Y., Qiu, J., Zhang, P., Zhang, J., Jiang, M. and Ma, Z. (2018). "Genetic variants in FAM13A and IREB2 are associated with the susceptibility to COPD in a Chinese rural population: a case-control study." Int J Chron Obstruct Pulmon Dis **13**: 1735-1745.

Zimmer, J. (2014). "Natural killers take on cancer." Nature **505**(7484): 483-483.

Zimmer, J., Ioannidis, V. and Held, W. (2001). "H-2D ligand expression by Ly49A+ natural killer (NK) cells precludes ligand uptake from environmental cells: implications for NK cell function." J Exp Med **194**(10): 1531-1539.

Ziółkowska-Suchanek, I., Mosor, M., Gabryel, P., Grabicki, M., Żurawek, M., Fichna, M., Strauss, E., Batura-Gabryel, H., Dyszkiewicz, W. and Nowak, J. (2015). "Susceptibility loci in lung cancer and COPD: association of IREB2 and FAM13A with pulmonary diseases." Scientific reports **5**: 13502.

Ziółkowska-Suchanek, I., Mosor, M., Podralska, M., Iżykowska, K., Gabryel, P., Dyszkiewicz, W., Słomski, R. and Nowak, J. (2017). "FAM13A as a Novel Hypoxia-Induced Gene in Non-Small Cell Lung Cancer." Journal of Cancer **8**(19): 3933.